Development of an Electrochemical Surface-Enhanced Raman Spectroscopy Aptasensor for the Early Detection of Acute Myocardial Infarction

By: Sam Michael Julien

A Thesis Submitted to

Saint Mary's University, Halifax, Nova Scotia

In Partial Fulfilment of the Requirements for the Degree of

Bachelor of Science with Honours in Chemistry

April 2022, Halifax, Nova Scotia

Supervisor: Dr. Christa Brosseau

Department Chair: Dr. Jason Masuda

Date: April 20, 2022

Certification

Development of an Electrochemical Surface-Enhanced Raman Spectroscopy Aptasensor for the Early Detection of Acute Myocardial Infarction

By: Sam Michael Julien

I hereby certify that this thesis was completed by Sam Michael Julien in partial fulfillment of the requirements of the Degree of Bachelor of Science with Honours in Chemistry at Saint Mary's University and I certify that this is truly the original work carried out by Sam Michael Julien.

Thesis Supervisor
Dr. Christa L. Brosseau

_____

Chairperson of the Chemistry Department

Dr. Jason D. Masuda

_____

Date: April 20, 2022

Abstract

Development of an Electrochemical Surface-Enhanced Raman Spectroscopy Aptasensor for the Early Detection of Acute Myocardial Infarction

By: Sam Michael Julien

A common cardiovascular disease is acute myocardial infarction (AMI), which is characterized as an ischemic event within the myocardium that results in irreparable damage to the heart. Unfortunately, current clinical methods lack sensitivity or are too time consuming to diagnose AMI events effectively. A common biomarker that is specific to AMI is the protein cardiac troponin I (cTnI). cTnI is a good protein biomarker for diagnosing AMI because it is part of the troponin complex which breaks down and is released into the blood stream when AMI events occur. The goal of this thesis was to build an aptamer-based biosensor (aptasensor) specific to cTnI using an electrochemical surface-enhanced Raman spectroscopy (EC-SERS) detection platform. EC-SERS was first used to prepare, optimize, and characterize a ternary (three component) monolayer consisting of an aptamer that specifically binds to cTnI, and two alkane thiols which backfill the surface and limit non-specific adsorption. Once optimized, the ternary monolayer was tested for blocking efficiency of non-target analytes, which was found to block >99% of non-target signal. This research also developed a new method for verifying the presence of the aptamer after the monolayer had been prepared using deuterated thiols. Finally, the ternary monolayer was tested for its aptasensing capabilities for the determination of cTnI, where no signal was detected for cTnI due to distance dependence issues that are a limitation of SERS techniques. Future work is needed to extend the applicability of SERS to aptamer-based sensors.

April 20, 2022

Acknowledgements

I would like to thank my research supervisor, Dr. Christa Brosseau for all her knowledge and guidance during the course of this project, her consistent encouragement and for providing me with the amazing work opportunities over the past summers. I would also like to thank the current and past Brosseau lab group members: Megan Himmelman, Carolyn Farling, Kaleigh McLeod, Tanner George, Maddison Eisnor, Mary Stackaruk, Sumayyah Chotoye, and Jaskaran Anand for being my mentors and colleagues who were always willing to help troubleshoot, and problem solve.

I would also like to extend my thanks to Elizabeth McLeod, Bitu Hurisso and Najwan Albarghouthi, as well as the entirety of the chemistry department staff for their ongoing support. I would like to thank the faculty in the department of chemistry for providing me with my education in chemistry and my appreciation for the subject.

Most of all I would like to thank my family and friends for their continued support and encouragement throughout this endeavor, specifically my sister Sylvie Julien and my partner Annie Michaud for always reminding me to think positive and push through the challenges.

Table of Contents **Page #**

List of Figures

List of Tables

List of Abbreviations

CVDs	Cardiovascular Diseases
AMI	Acute myocardial infarction
cTnI	Cardiac troponin I
cTnT	Cardiac troponin T
cTnC	Cardiac troponin C
ELISA	Enzyme Linked Immunosorbent Assay
ECG	Electrocardiogram
POC	Point-of-care
SELEX	Systematic evolution of ligands by exponential enrichment
SERS	Surface-enhanced Raman spectroscopy
EC-SERS	Electrochemical surface-enhanced Raman spectroscopy
PVD	Physical vapor deposition
SAM	Self-assembled monolayer
NP	Nanoparticle
AgNP	Silver nanoparticle
DNA	Deoxyribonucleic acid
RNA	Ribonucleic acid
A	Adenine
T	Thymine
G	Guanine
C	Cytosine

AMD	Acute macular degeneration
Anti-VEGF	Anti-vascular endothelial growth factor
ssDNA	Single stranded DNA
ssRNA	Single stranded RNA
PCR	Polymerize chain reaction
12-MDA	12-mercaptododecanoic acid
ATP	Adenosine triphosphate
LSPR	Localized surface plasmon resonance
IHP	Inner Helmholtz plane
OHP	Outer Helmholtz plane
OCP	Open circuit potential
WE	Working electrode
RE	Reference electrode
CE	Counter electrode
Ag/AgCl	Silver/silver chloride reference electrode
CV	Cyclic voltammetry
TCEP	Tris(2-carboxyethyl) phosphine
R6G	Rhodamine 6G

Chapter 1: Introduction

1.1 Preamble

Cardiovascular Diseases (CVDs) remain the leading cause of death worldwide each year.[1] CVDs are the second most common cause of death in Canada killing approximately 12 adults over the age of 20 each hour.[2] One common CVD is acute myocardial infarction (AMI), which is characterized by a lack of blood supply and therefore lack of oxygen in the myocardium.[3] This event is known as ischemia and results in irreparable cell death.[3] The four common biomarkers of CVD that are released into the blood stream during cardiac events are thrombin, myoglobin, creatine kinase MB and cardiac troponins.[3] Cardiac troponins are further differentiated into cardiac troponin I (cTnI), cardiac troponin T (cTnT) and cardiac troponin C (cTnC). Of these biomarkers, cTnI is considered the "gold standard" for diagnosing AMI events because it is highly specific to AMI events and it persists in the blood stream for up to 10 days following an AMI event.[4,5] In a healthy adult, cTnI levels are approximately 0.4 ng/mL, however in an individual who has experienced an AMI event, levels of cTnI will be elevated above 2 ng/mL.[5]

Current clinical detection methods of AMI events include enzyme linked immunosorbent assays (ELISA) and electrocardiograms (ECG).[3] While ELISA is capable of detecting levels of cTnI as low as 10 pg/mL, it must be completed in a central laboratory and is very time consuming, taking up to 6 hours to complete an analysis of a blood sample.[3] In contrast, an ECG is very fast at diagnosing heart attacks but lacks the sensitivity needed to diagnose acute heart failure events like AMI.[3] It is therefore evident that a test be developed for a clinical setting that can diagnose AMI in a sensitive, selective and rapid manner.

Aptamers are an oligonucleotide sequence (single stranded DNA or RNA) isolated through a process known as the systematic evolution of ligands by exponential enrichment (SELEX) which can bind selectively to a target.[6,7] Further, they are specifically engineered to have high binding affinities towards a specific target, are easily modified and are more robust than a traditional antibody.[5,8] For these reasons, in the past 20 years, there has been extensive research into the development of aptamer-based biosensors (aptasensors).[9,10]

In 2015, the first aptamers specific to the protein cTnI were isolated.[11] Since then, numerous aptasensors have been developed in an attempt to develop a point-of-care (POC) test for AMI in a clinical setting. Aptamers are oligonucleotide sequences of single stranded DNA or RNA that have high binding affinities for a specific target.[6,7] In recent years, it has been argued that aptamers are a better choice than antibodies for biosensing due to the fact that aptamers do not need an animal host, they are easily modified and they are easily synthesized.[7,12] In addition, aptamers can be designed to bind to a wider variety of targets, ranging from ions to molecules to proteins to entire cells.

Many aptasensors have been developed to detect cTnI quantitatively.[5,11] Some of the detection methods used in currently developed aptasensors include differential pulse voltammetry, electrical impedance spectroscopy, chemiluminescence and SERS.[6,12] For the majority of the cTnI aptasensors that have been previously developed, the Tro-4 aptamer is the most common aptamer choice because it possesses a very high binding affinity for the protein biomarker cTnI.[11] Overall, the binding constant (K_d) for the Tro-4 aptamer binding cTnI was found to be 270 pM.[11]

Electrochemical surface-enhanced Raman spectroscopy (EC-SERS) is a promising detection platform for developing a cTnI aptasensor. Raman spectroscopy is a vibrational spectroscopy technique that uses the inelastic scattering of monochromatic light.[13,14] Although the

Raman signal is inherently weak because only 1 in 10^6 photons scatter inelastically, when coupled to a plasmonic material such as nanostructured silver, localized surface plasmon resonance (LSPR) is generated from the conduction electrons of the nanoparticle.[13,15] Further, hot spots are created when nanoparticles aggregate very close together, leading to Raman signal enhancement of up to 10^6.[13] The Raman signal can be enhanced even further when it is coupled with electrochemistry as the applied potential is capable of bringing analytes closer to the plasmonic surface, maximizing the enhancement even further.[13,16]

There are two ways to prepare a SERS substrate, the bottom-up method and the top-down method.[17] With a top-down approach, a plasmonic substrate is prepared by some sort of deposition process such as physical vapor deposition (PVD).[18,19] In contrast, a bottom-up method of preparing a SERS substrate prepares plasmonic materials (nanoparticles) through chemical reactions, and then the nanoparticles are assembled onto the surface.[18] When dealing with complex analytes, the substrate typically has to be functionalized in order to block non-target species from adsorbing to the surface, which can be accomplished by preparing a self-assembled monolayer (SAM).[16,20,21] A self-assembled monolayer (SAM) is a method for modifying the surface of a plasmonic substrate that increases the number of reporters (aptamer molecules) on the substrate and overcomes the barrier of gross aggregation on a NP surface.[20] SAM probes are typically prepared by attaching molecules that contain a thiol group to the NP surface.[20] The thiol group acts to bind to the metal surface as it is capable of forming strong Ag-S bonds.[20] Advantages of SAM's include high surface coverage with reporter molecules, uniform orientation of the reporters giving reproducible results, high surface coverage which reduces the possibility of co-adsorbing analytes that will interfere with the analyte of interest, and ease of multiplexed testing as various reporters can be attached in this fashion.[20]

For this work, a bottom-up method was used, first by synthesizing silver nanoparticles (AgNPs) and coating carbon screen printed electrodes with these AgNPs. Next, a self-assembled ternary (three-component) monolayer was prepared on the plasmonic substrate. These three components included a thiol-modified Tro-4 aptamer, and two alkane-thiols to backfill and block non-specific adsorption. Finally, the aptasensor was tested for proof-of-concept qualitative performance using recombinant cTnI at a concentration of 250 μg/mL.

1.2 Objectives of this Thesis

The objectives of this thesis were as follows:

- Development and optimization of a ternary (three-component) monolayer containing the Tro-4 aptamer and two alkane thiols
- Verification that non-specific adsorption was blocked by the ternary monolayer
- Method optimization for reduction of the aptamer linker
- Development of a method for verifying the aptamer was still present after ternary monolayer preparation
- Obtaining electrochemical surface-enhanced Raman (EC-SERS) spectra of pure cardiac troponin I (cTnI)
- Qualitative testing of the efficacy of the prepared aptasensor for cTnI detection

1.3 Scope of this Thesis

This thesis contains 8 chapters, and each chapter contains the following information. Chapter 1 is an introduction to this project and contains a short preamble, goals of this thesis work and a summary of what is contained in this thesis. Chapter 2 is a background chapter containing a full literature review, as well as the relevant background theory needed to understand this work.

Chapter 3 contains all methods used for this research. Chapter 4 contains the prominent results of this work. Chapter 5 contains the conclusions of this research. Chapter 6 contains directions for future work for this project. Finally, Chapter 7 contains all references for this work and Chapter 8 contains the appendix which includes supplementary data as well as copyright permission letters.

Chapter 2: Background

2.1 Literature Review

2.1.1 Cardiovascular Disease

Cardiovascular Diseases (CVDs) remain the leading cause of death worldwide, accounting for an estimated 31% of deaths each year.[1] Acute myocardial infarction (AMI) is one of the most common CVDs. AMI occurs when there is ischemia within the myocardial tissue, which is a lack of blood supply, and therefore lack of oxygen in the myocardium.[4,3]

Commonly, the symptoms of a cardiovascular event can include pain or discomfort in the chest, pain or discomfort in the arms, left shoulder, back, or jaw.[1] Furthermore, CVD patients can experience shortness of breath, nausea, light-headedness, a cold sweat, and pale colouration.[1] Symptoms of CVDs are known to present differently between men and women, therefore the best way to truly diagnose CVDs is through biomarkers in the blood.[1,3]

Four common biomarkers of CVDs that are released into the bloodstream during cardiac events are thrombin, myoglobin, creatine kinase myocardial band (CK-MB), and cardiac troponins.[3] Cardiac troponins are further differentiated into cardiac troponin I (cTnI), cardiac troponin T (cTnT) and cardiac troponin C (cTnC). Of these biomarkers, cTnI is considered the "gold standard" for diagnosing AMI events because it is highly specific to AMI events and it persists in the bloodstream for up to 10 days following an AMI event.[4,5] In a healthy adult, cTnI levels are approximately 0.4 ng/mL, however in an individual who has experienced an AMI event levels of cTnI will be elevated above 2 ng/mL.[5]

Current methods of testing for CVDs lack the sensitivity to diagnose more acute heart failure events like AMI, or are too time consuming to diagnose AMI in a timely manner before more

serious heart failure occurs.[3,5,11] The most common method for heart attack detection is an electrocardiogram (ECG), which delivers a rapid result based on electrical impulses from the heart, but is not sensitive enough to detect smaller heart issues like AMI.[3,5] In contrast, highly sensitive methods like enzyme linked immunosorbent assays (ELISA) are capable of detecting levels of cardiac biomarkers in blood as low as 10 pg/mL, but need to be carried out in a central laboratory and can be prohibitively expensive and time consuming.[3]

2.1.2 DNA

The structure of deoxyribose nucleic acid (DNA) was discovered to be a double helix in 1953.[22] DNA is comprised of the four heterocyclic nitrogen bases adenine (A), thymine (T), cytosine (C), and guanine (G).[22] A nucleotide base consists of the nitrogen heterocycle (nucleotide base), a deoxyribose sugar (contains a hydrogen instead of an OH in the C2 position), and a phosphate group on the C5 of the sugar.[22] These nucleotides form phosphodiester bonds between the phosphate and the OH on the C3 carbon of the deoxyribose sugar, which is why DNA terminal ends are denoted 5' (the C5 phosphate end) and 3' (the C3 OH end).[22] As shown in Figure 1, DNA forms hydrogen bonds between A-T and G-C nucleotides between complimentary strands of the double helix.

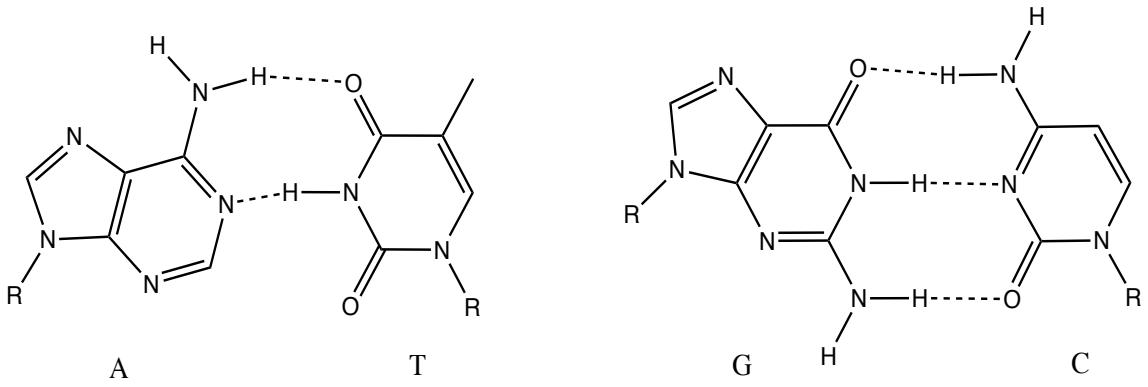

Figure 1. Schematic of the base pairings and hydrogen bonding pattern of DNA

Since the discovery of the double helical structure of DNA, there has been increased research into the field of DNA-based sensors. While there have been some successfully developed applications, the DNA often has to be modified with labels, which negatively affects the sensitivity of the sensor and makes the method very expensive.[23] In recent years, efforts have been made to develop label-free detection of molecules using DNA, which has since been widely applied using various detection techniques such as voltammetry, electrical impedance spectroscopy, amperometry and Raman spectroscopy.[16,24]

2.1.3 Aptamers

In 1990, three different groups simultaneously described aptamers as synthetic single stranded nucleic acid sequences (ssDNA or ssRNA) which bind selectively to a target.[25–27] Aptamers adopt very stable secondary structures, which permit them to interact with analytes which can range from ions to molecules to proteins or even whole cells.[6,8,28] Aptamers are specifically engineered to have high binding affinities towards a specific target such as a protein, lipid, small molecule or another DNA fragment.[5,8] Furthermore, the high binding affinities (1.0 pM – 1.0 μM) of aptamers allows them to achieve detection limits in the picomolar range for large targets and micromolar ranges for small molecules.[8]

Recently, aptamers have been widely used for both analytical and biological applications such as target capture, cell imaging, drug delivery, and molecular sensing.[29] Some of the most widely studied aptamers from the literature include the thrombin and PEGaptanib© aptamers.[30] PEGaptanib© is a therapeutic drug used for acute macular degeneration (AMD) that received FDA approval in 2004 and uses an anti-VEGF (vascular endothelial growth factor) aptamer.[30] VEGF 165 causes abnormal blood vessels to grow in the eyes, which leads to blood leakage and eventual vision loss.[30] The anti-VEGF aptamer is injected into the patient's vitreous cavity to bind to the target, inhibiting the binding between the target and its receptor.[30] Overall, this therapeutic aptamer has been shown to significantly improve vision of patients, and has since been widely applied as treatment for AMD as well as for diabetic retinopathy (DR).[30]

To isolate a highly selective and highly sensitive aptamer, it is necessary to have a very careful process in which aptamers are prepared. Although aptamers were discovered by three groups simultaneously, the ideal isolation method for synthetic aptamers was only described by two different groups independently, and the process became known as systematic evolution of ligands by exponential enrichment (SELEX).[26,27] SELEX consists of first preparing a random pool of ssDNA or ssRNA, binding the target, eluting the sequences that bind to the target and finally an amplification step is used to concentrate the desired target sequence.[8,30] The random ssDNA pool contains approximately 10^{15} unique nucleotide sequences; each sequence consisting of a random central sequence and a defined sequence on both the 5' and 3' ends.[7] The random pool is then incubated with the target molecule where some sequences will bind strongly to the target and others will be weakly bound or completely unbound to the target.[30] The enriched pool is then eluted from the bulk pool using various separation techniques such as affinity chromatography, or capillary electrophoresis.[7] The eluted aptamers are then amplified using polymerase chain reaction

(PCR) which binds to PCR primers in the defined sequence region of the aptamers.[7] This cycle is then repeated 8-12 times in order to obtain an aptamer that is highly sensitive and specific towards the target molecule.[7,30] A full schematic of the SELEX process is shown in Figure 2 below.

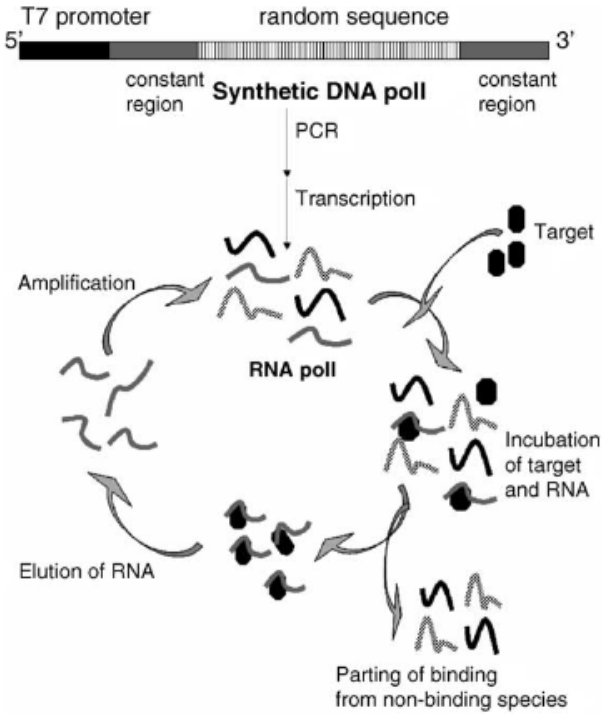

Figure 2. Flow chart depicting the SELEX process where aptamers are selected from the random ssDNA pool, eluted and amplified. (Reproduced with permission[7])

Although the process of SELEX remains the most widely used method of aptamer isolation today, a major limitation of the technique is that it takes multiple weeks to complete the process. Due to this limitation, efforts were made to make the process faster, which includes coupling it with other techniques: photo-SELEX, capillary electrophoresis-SELEX, and microfluidic-SELEX.[7,29] In addition, there have also been non-SELEX processes developed for the isolation of aptamers, namely capillary electrophoresis and non-equilibrium capillary electrophoresis of an equilibrium mixture.[29,31]

The first aptamers specific to the cardiac biomarker cTnI were isolated in 2015.[11] In short, the SELEX process was applied and six different DNA sequences with high binding affinities for cTnI were fully characterized. The most selective and sensitive of these aptamer sequences was the Tro-4 sequence which is shown below in Figure 3.[11] Since then, numerous aptasensors have been developed using different sensing platforms, but the Tro-4 aptamer is the most highly used sequence for designing a biosensor for the detection of cTnI.[6,12,28]

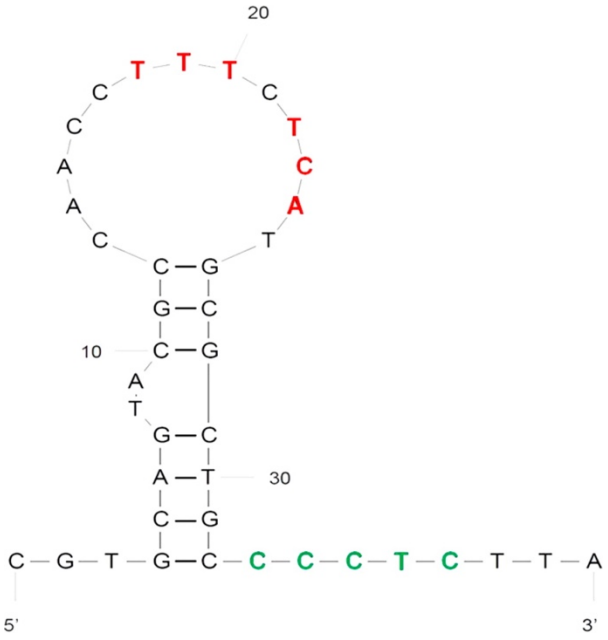

Figure 3. Depiction of the Tro-4 aptamer structure (Reproduced with permission[11])

2.1.4 Aptasensors

In the past twenty years, there has been extensive research into the development of DNA-based biosensors.[9,10] Many current DNA-based biosensors make use of aptamers, and are therefore named aptasensors. As previously mentioned, aptamers are highly selective and sensitive towards a specific target molecule which makes them extremely useful for rapid detection of viruses, bacteria, proteins or other chemical substances.[7,9]

Another reason why aptasensors are a very promising method for future diagnostic testing is that they offer numerous advantages in comparison to traditional antibody-based sensors.[9,12] Aptamers are desirable because they are more robust and more easily synthesized and modified in the lab in comparison to antibodies which require a host organism to grow, cannot be easily modified and are conformationally susceptible to temperature and pH changes.[7,12] Currently, aptasensors have been applied to various analytical techniques including voltammetry, surface-enhanced Raman spectroscopy (SERS), electrochemical SERS (EC-SERS), and chemiluminescence sensors.[7,12,16] In the literature, some applications of aptasensors include the diagnosis of tuberculosis and the quantification of cardiac biomarkers such as thrombin, myoglobin and cTnI.[3,16] The first cTnI aptasensor was developed by Jo et al. in 2015. As previously mentioned, this study isolated six different aptamers that possessed high binding affinities toward cTnI. Of these aptamers, the one with the highest binding affinity was the aptamer named Tro-4 which was used to build an aptasensor that detected cTnI using square wave voltammetry with a linear dynamic range of 1 – 10,000 pM.[11]

The most important part of designing an aptasensor is choosing the best sequence (highest binding affinity for cTnI) for the analyte of interest: for this thesis work the Tro-4 aptamer was used. The other important aspect is ensuring the aptamer is properly immobilized to the surface of the sensor such that the aptamer can properly interact with the molecule of interest.[32] To ensure the aptamer is properly oriented on the sensor surface, the strong chemisorption properties of thiols to silver substrates is often taken advantage of in order to prepare what is known as a self-assembled monolayer (SAM).[20] Self-assembly is useful for building an aptasensor because aptamers can be easily modified to contain various functional groups on either the 5’ or 3’ end, including thiol groups.[7] For a SAM, the specific functional group of interest is a thiol (-SH)

because thiols form strong metal – sulfur bonds which optimizes the surface coverage of the aptamer, as well as reduces the likelihood of the aptamer becoming physisorbed to the substrate.[20] Furthermore, alkanethiols can be immobilized onto the surface in order to "backfill" the surface after the aptamer has been immobilized which limits non-specific adsorption of non-target species.[16,21] A schematic for the aptasensor SAM, a three-component, or ternary monolayer, prepared in this work can be seen in Figure 4 below.

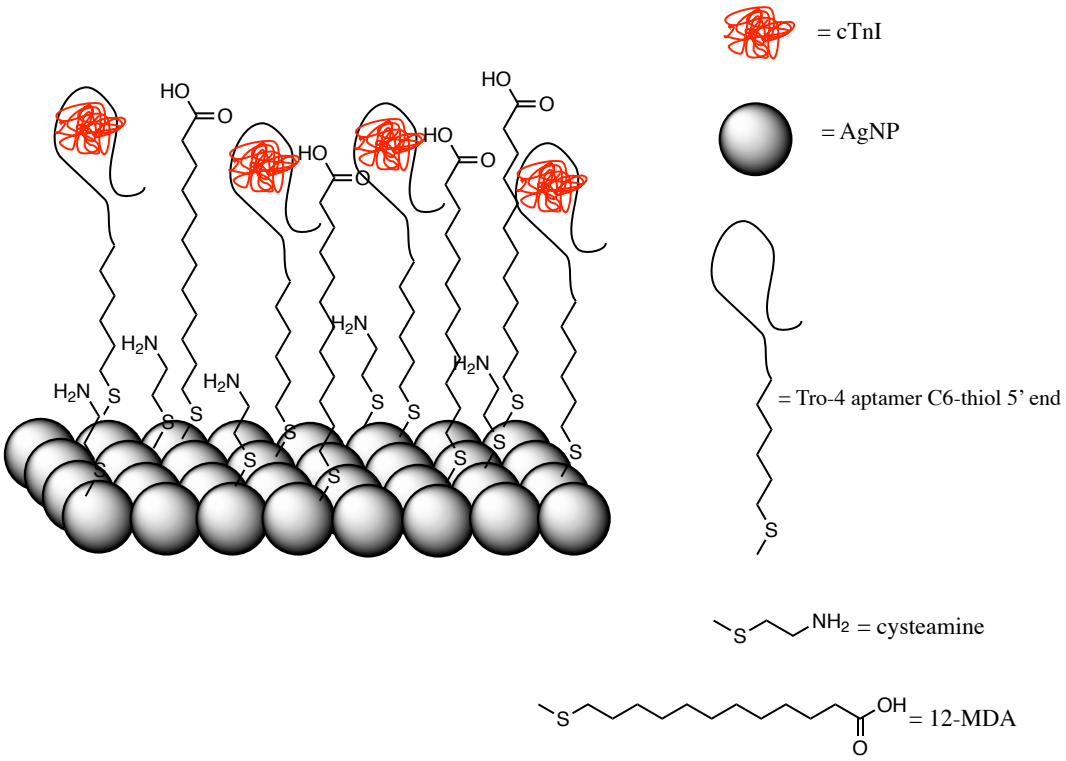

Figure 4. Schematic of the Tro-4 aptamer immobilized on the AgNP surface with 12-MDA and cysteamine immobilized as backfilling agents.

2.1.5 SERS Based Aptasensors

As previously mentioned, aptamers can be used for the detection of many targets including viruses, proteins, and bacteria.[7,9] Aptasensing is still a growing field, but in recent years, many

surface-enhanced Raman spectroscopy (SERS) based aptasensors have been developed. Some of the most successful SERS-based aptasensors include a SERS aptasensor for the detection of salmonella and staphylococcus, as well as a SERS-based aptasensor for the detection of exozomes.[33,34]

Furthermore, SERS-based aptasensing has been used to detect biomarkers of tuberculosis, cardiac biomarkers, as well as hormones and neurotransmitters.[12,16,35] Some noteworthy examples of successful SERS-based cardiac biomarker detection include the development of cTnI aptasensors and numerous developed SERS-based aptasensors for the detection of the cardiac biomarker thrombin which activates fibrinogen, fibrin and platelets which cause clotting of the blood.[12,36–38] Another noteworthy mention of a SERS-based aptasensor is the development of an aptasensor for the quantification of dopamine. Dopamine is a neurotransmitter that regulates numerous physiological pathways and is essential for brain function.[35] The group of Tang et al. was able to quantify levels of dopamine with a linear dynamic range from 0.01 – 10 pM which highlighted SERS-based aptasensing as a potentially promising technique for the diagnosis of dopamine-deficiency diseases such as Parkinson's Disease.[35]

Overall, with aptasensing being a growing field, it is expected that many more useful applications of SERS-based aptasensors will be developed in the future because SERS is a highly sensitive technique capable of single molecule detection.[39]

2.1.6 Cardiac Troponin I

As previously mentioned, cardiac troponin I (cTnI) is considered the "gold standard" for CVD diagnosis via detection of biomarkers. However, it is important to understand what cTnI is and what it does in the body.[4] In a healthy individual, cTnI is part of a quaternary protein known

as the troponin complex.[40–42] This complex can be seen in Figure 5 and its function is to regulate muscle contractions of the heart.[42]

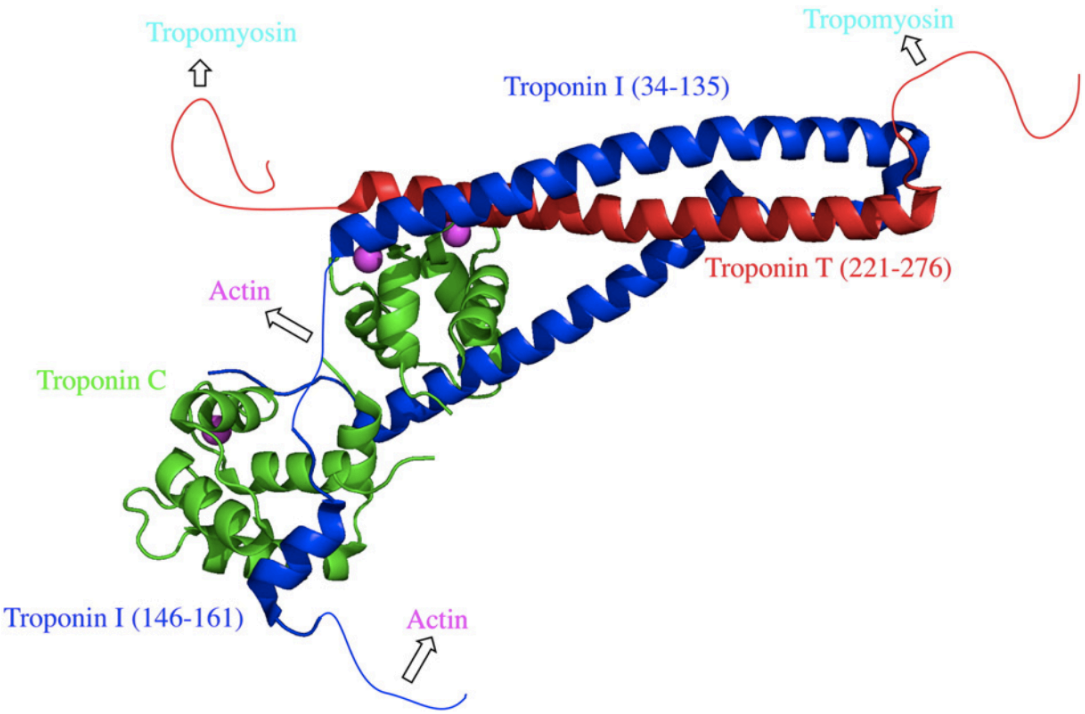

Figure 5. X-ray crystallography structure of the troponin complex. (Reproduced with permission[43])

The troponin complex regulates cardiac muscle contraction by regulating the influx of Ca^{2+} and inhibiting ATP activity by the cTnI (inhibitory) subunit binding to ATP.[42] This inhibition of ATP regulates the cycle of the actin-myosin motor where Ca^{2+} binds to tropomyosin and ATP hydrolysis causes muscle recovery.[22,42]

Acute myocardial infarction (AMI) causes the troponin complex to breakdown (cardiomyocyte necrosis) and results in the cardiac muscle being improperly regulated.[42] When cardiomyocyte necrosis occurs, the different components (cTnI, cTnT, and cTnC) are released into the bloodstream.[3,42] It is for this reason that elevated levels of cTnI detected in the blood is a very

good early indicator of AMI or some other acute heart failure, because it indicates that the cardiac muscle will be susceptible to improper contractions due to the lack of Ca^{2+} and ATP regulation.[42,43]

2.2 Theory

2.2.1 Raman Spectroscopy

Raman spectroscopy is a widely used vibrational spectroscopy technique that provides qualitative information about an analyte based on the unique vibrational fingerprint of that molecule.[44] Raman scattering was first described in 1928 by Chandrasekhara Venkata Raman and Kariamanikkam Srinivasa Krishnan.[14] Raman spectroscopy makes use of the inelastic scattering of monochromatic light that occurs when an incident beam is focused onto a sample.[32,44] Rayleigh scattering is elastic scattering and makes up the majority of the scattering of the incident beam.[45,46] In contrast, both Stokes and anti-Stokes scattering are inelastic forms of scattering (Raman scattering). When the frequency of relaxation is less than the frequency of the incident light, Stokes scattering arises.[44–46] When the frequency of relaxation is more than the frequency of the incident light, anti-Stokes scattering is the result.[45,46] A visual depiction of Raleigh scattering, Stokes scattering and anti-Stokes scattering can be seen in Figure 6.[45]

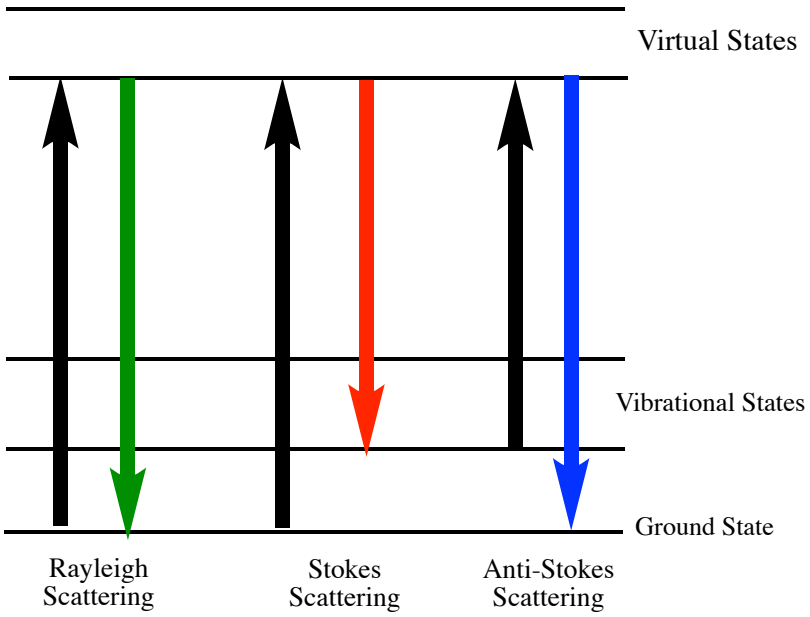

Figure 6. Depiction of the different scattering modes of monochromatic light: Rayleigh, Stokes and anti-Stokes

An advantage of Raman spectroscopy is that in comparison to IR spectroscopy (another vibrational technique) spectral contributions from water, carbon dioxide and glass are modest at best, which allows researchers to conduct studies in aqueous media in glass containers without interference.[45,47] Raman spectroscopy is also a non-destructive technique, making it an ideal technique for characterizing biological systems, as well as delicate materials such as art samples.[16,20,48] Furthermore, Raman spectroscopy is a very simple technique that requires only small amounts of sample that often need little to no sample preparation beforehand, and the analysis time is very fast.[16,46,49]

A major limitation of normal Raman spectroscopy is that it is an inherently weak technique because only 1 in ~10^6 photons scatter inelastically.[45,46,50] For this reason, Raman spectroscopy was not widely applied until the 1970s when lasers and more sensitive photon detectors became available.[50]

2.2.2 Surface-Enhanced Raman Spectroscopy (SERS)

Due to the inherently weak signal of normal Raman spectroscopy, this technique lagged behind infrared spectroscopy as a vibrational characterization tool until further advancements were demonstrated. This was achieved in 1974, when Fleishman et al. recorded the enhanced Raman spectrum of pyridine on roughened silver. However, at the time of this study it was not fully understood why the signal was enhanced, with the authors attributing it to the increased surface area of the roughened silver.[39] It was not until 1977, however, that Surface-Enhanced Raman spectroscopy (SERS) was discovered by two separate research groups: the group of Van Duyne and Jeanmaire as well as the group of Albrecht and Creighton.[51,52] Surface enhancement occurs due to both electromagnetic and chemical factors, but the electromagnetic component accounts for the bulk of the enhancement.[53] The electromagnetic enhancement is due to the interaction of the incident beam of light with the conduction electrons of a coinage metal such as silver, gold, or copper which results in a process known as localized surface plasmon resonance (LSPR).[39,53,54] LSPR occurs when the conduction electrons experience quantum confinement within the dimensions of the metal nanosphere, and the electrons oscillate in response to the oscillating electric field of the incident light, resulting in a very strong electromagnetic field at the nanostructured surface.[55] A schematic of LSPR is shown in Figure 7 where the conduction electrons of the metal nanosphere interact with the incident light in a collective oscillatory manner.

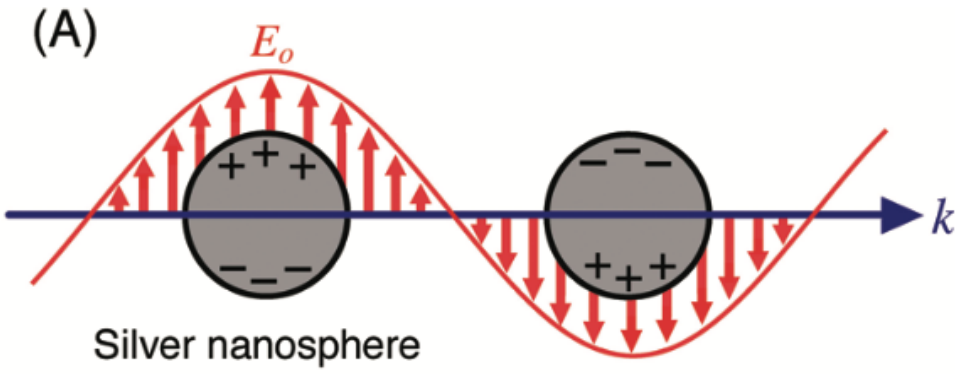

Figure 7. Depicts the interactions of the free electrons of the nanosphere with the electric field of the incident beam.[55] Reproduced with permission

The increased intensity of the electromagnetic field leads to a greater induced dipole for the analytes and more inelastic scattering.[17,54] An induced dipole (Van der Waals force) is the instantaneous dipole that is created when the electron cloud of a molecule becomes concentrated at a given area due to interaction with other molecules or in the case of Raman spectroscopy, the interaction of the analyte with the electromagnetic field.[56] The enhancement is even further increased when two nanoparticles are in very close proximity (typically within 1 nm) or when sharp features such as the points of nanostars are present.[17,55] The significant local field enhancement observed at nanoparticle junctions and sharp features are known as "hot-spots".[17,53] The increase of inelastic scattering results in an enhanced signal orders of magnitude greater (up to 10^{12}) than the normal Raman signal.[39,54] Rather than using neat liquids or pure powders of analyte, SERS can be applied when more sensitive analytical methods are needed, such as for biosensing.[20,48] Most SERS substrates make use of the coinage metals such as silver, gold and less commonly, copper.[39,55] These metals are ideal because they are relatively stable and they display optimal plasmonic properties over a wide range of visible and near infrared wavelengths, as shown in Figure 8.[39]

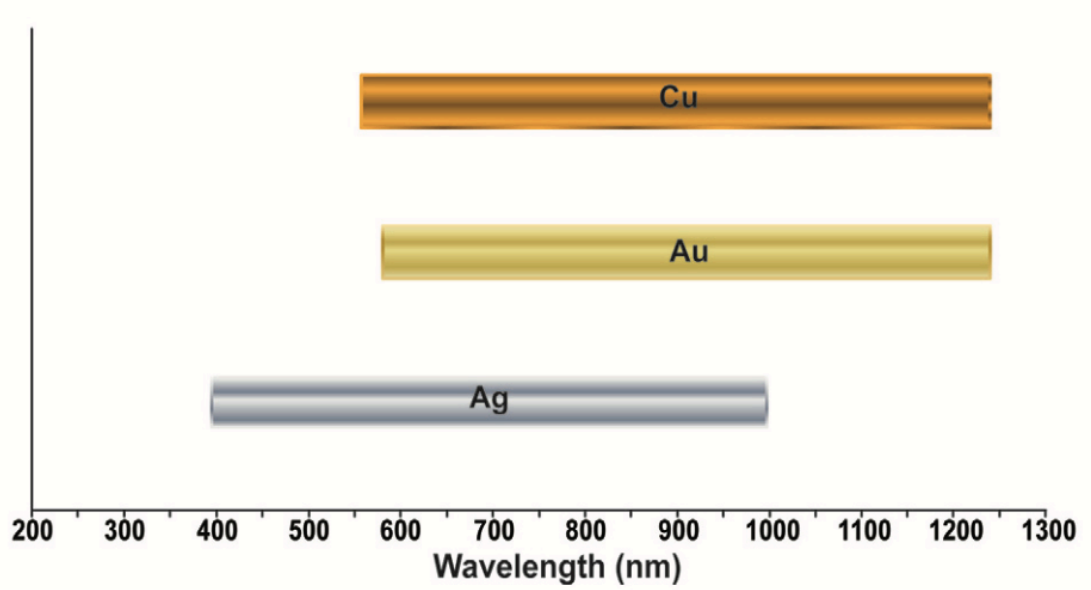

Figure 8. Depiction of the LSPR ranges for the ideal SERS substrates of silver, gold and copper.[39] (Reproduced with permission)

2.2.3 Electrochemistry

Electrochemistry is the study of how electricity affects different chemical interactions and reactions.[57] Electrochemistry has been widely used in applications such as biomedical analysis, quality control in industry and battery fuel cells.[57] Electrochemical processes take place at the electrode-solution interface and the method varies based on the type of electrical signal used for detection of analyte.

Electrochemical applications can be grouped into two prominent methods: potentiometric and potentiostatic. Both techniques use electrochemical cells, which consist of at least two electrodes and an aqueous salt solution that conducts electricity (known as the supporting electrolyte).[57] The electrolyte used is chosen based on solubility of the analyte, electrical conductivity, and electrochemical stability.[57] An ideal electrolyte ranges in concentration from

0.1-1.0 M and has a high ionic strength, which decreases the solution resistance and prevents migration.[57] One issue with aqueous electrolyte solutions is that they absorb oxygen from the atmosphere, which causes problems when conducting electrochemical studies. One way to limit this effect is to purge the electrolyte of oxygen by bubbling the solution with an inert gas, such as argon, before use.[57] Potentiostatic methods investigate the charge transfer process at the interface of the electrode and the solution.[57] The electrode potential is used to probe electron-transfer processes between the analyte and electrode, resulting in a net current which can be measured.[57] Potentiostatic methods measure chemical species that can participate in oxidative and reductive processes, which makes them easily applicable to the development of highly sensitive, selective, portable, and cost-effective techniques.[57] When under potentiostatic conditions, electrodes develop a surface charge attracting ions from solution of the opposite charge which leads to the formation of an electrical double layer shown schematically in Figure 9.[58] The double layer consists of a diffuse layer and a compact layer, which is further divided into the inner Helmholtz plane (IHP) and the outer Helmholtz plane (OHP).[58] The inner Helmholtz plane (IHP) is the layer closest to the electrode surface and contains fully adsorbed ions, which can be adsorbed via covalent or van der Waals forces.[58] The outer Helmholtz plane (OHP) is an imaginary plane passing through the center of solvated and non-specifically adsorbed ions.[58] The diffuse layer is a gradient of charge accumulation extending from the outer Helmholtz plane to the bulk solution.[58]

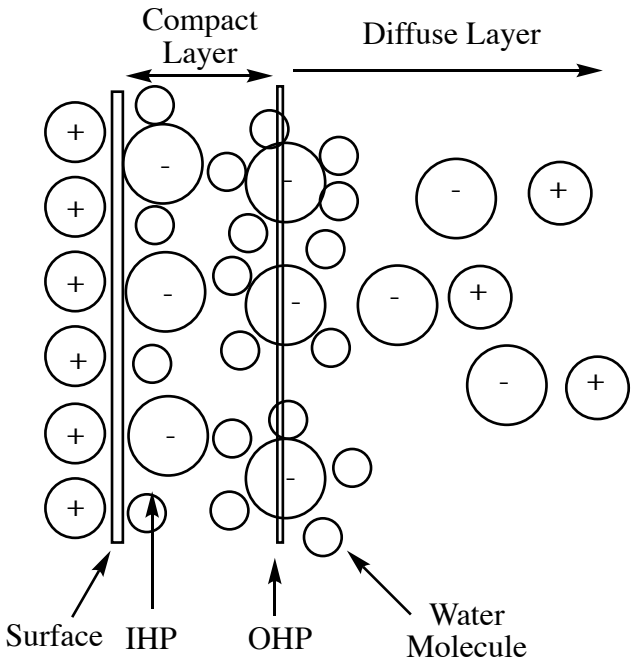

Figure 9. Schematic of the Grahame model electrical double layer (adapted from[58])

When conducting electrochemical studies where the potential is controlled, the electrochemical cell contains three electrodes: a working electrode (WE), a reference electrode (RE) and a counter electrode (CE).[57] The WE is where the electrochemical process of interest occurs.[57] The RE is held at a constant potential, the most common RE being a silver-silver chloride (Ag/AgCl) electrode.[57] The CE allows for the measurement of the potential of the working electrode while passing current.[57]

2.2.4 Electrochemical Surface-Enhanced Raman Spectroscopy (EC-SERS)

While SERS uses coinage metals in order to obtain extensive enhancement of Raman signals, electrochemistry can be coupled to SERS, which is given the name electrochemical surface-enhanced Raman spectroscopy (EC-SERS).[59] The change in electrical potential of the SERS substrate *in situ* has been shown to increase the already highly enhanced sensitivity of SERS.[16,59]

EC-SERS measures the Raman spectra of the molecules adsorbed to the surface of an electrode, and monitors changes as a result of applied voltage or current.[59] These changes can include complete adsorption or desorption of molecules, or electrochemical conversion into other molecular species, which can allow for multi-analyte analysis.[59,60]

When conducting regular SERS analysis, the strong electromagnetic field created by the LSPR of the substrate accounts for the majority of the enhancement, but in EC-SERS the chemical enhancement mechanism plays a more significant role.[61] Chemical enhancement is caused by various processes such as chemisorption interactions, and photon-driven charge transfer between the adsorbed analyte and the substrate.[61]

EC-SERS can be applied as a sensitive, simple, cost-effective, and portable detection platform.[16,59] Furthermore, EC-SERS allows the analyte to be closer to the surface, which is advantageous because SERS is a highly distance-dependent technique in which maximum SERS signals are observed when the analyte if less than 5 nm from the enhancing surface.[17,55] As well, by applying a potential, different analytes can adsorb and desorb from the substrate surface which allows for multi-analyte detection.[60] As such, EC-SERS has been applied as a sensitive method for the detection of biological molecules, DNA aptamers, drug metabolites and art sample analysis.[16,60,62] It is therefore clear why EC-SERS is a desirable platform for the development of an aptasensor for the detection of cTnI and diagnosis of AMI.

Chapter 3: Experimental

3.1 Reagents and Materials

Potassium phosphate dibasic (≥98%) was purchased from Anachemica Canada (Montréal, QC, CA), potassium phosphate monobasic (≥99%), 12-mercaptododecanoic acid (12-MDA) (96%), cysteamine (>98%), potassium chloride (≥99%), guanine (98%), adenine (≥99%), thymine (≥99%), cytosine (≥99%), $NaBH_4$ (≥99%), tris(2-carboxyethyl)phosphine hydrochloride (TCEP) (≥98%) and rhodamine 6G (95%) were purchased from Sigma-Aldrich (St, Louis, MO, USA). Sodium citrate was purchased from ACP Chemicals (Montréal, QC, CA). Silver nitrate (99.9995%) and citric acid (99+%) were purchased from Alfa Aesar (Ward Hill, MA, USA). 2-aminoethane-d_4-thiol HCl (99%) and 1-dodecane-d_{25}-thiol (98%) were purchased from CDN Isotopes (Pointe-Claire, QC, CA). Details regarding the DNA oligonucleotide for this work are as follows: The Tro-4 aptamer sequence was modified at the 5' end to contain a 6-carbon thiol linker to allow for the aptamer to be easily immobilized to the substrate surface via a Ag-S bond where the D denotes that the thiol was shipped as a more stable disulfide.

Tro-4 Aptamer:

5'-/5ThioMC6-D/-CGTGCAGTACGCCAACCTTTCTCATGCGCTGCCCCTCTTA-3'

was purchased from Integrated DNA Technologies Canada (Toronto, ON, CA). Recombinant cardiac troponin I protein (>95%) was purchased from MyBioSource (San Diego, CA, USA). Aside from the Tro-4 aptamer which was reduced to its SH form by TCEP, and the cTnI protein which was diluted with pH 7.4 phosphate buffer to specific concentrations, all chemicals were used as received without further purification. All solutions were prepared using Millipore water (resistivity ≥ 18.2 MΩ cm). All glassware was soaked in neat sulfuric acid overnight and rinsed

30 times with Millipore water. Screen printed electrodes (SPEs) used to prepare the EC-SERS substrates and the WaveNow Potentiostat/Galvanostat System were purchased from Pine Research Instrumentation (Durham, NC, USA).

3.2 Nanoparticle Synthesis and Characterization

Silver nanoparticles were synthesized using a modified Lee-Meisel method.[62,63] 1.0 mL of aqueous silver nitrate solution (0.1 M), 3.4 mL of aqueous sodium citrate (5 % w/v), and 0.6 mL of aqueous citric acid (0.17 M) are added into a 250 mL three-neck flat-bottom flask with 95.0 mL of Millipore water. 0.2 mL of freshly prepared sodium borohydride solution (0.1 mM) was then added into the above mixture at room temperature under magnetic stirring. The mixture was allowed to stand at room temperature for 1 min and then brought to boil under reflux within 20 min under magnetic stirring. After boiling under reflux for 1 h, the heat was turned off and the dark yellow solution was allowed to cool to room temperature while stirring for 1h. To concentrate the AgNPs, aliquots of 16 × 1.40 mL of colloidal suspension were added to Eppendorf tubes, which were then centrifuged at 8 000 rpm for 20 min using a Mandel Benchmark MC-24 touch microcentrifuge (Guelph, ON, CA). The supernatant was then removed and discarded, and the remaining pellet was placed into one tube and centrifuged again. The volume of the final AgNP paste was determined and made up to 50 μL with Millipore water. This was repeated as many times as necessary for each batch of AgNPs. The AgNPs were characterized by UV-vis looking for the distinct peak at 390 nm and by SEM in order to verify the AgNP were uniform in size and approximately 30 nm in diameter as seen in the appendix Figure A5.

3.3 Spectroscopic Studies

Ultraviolet-visible (UV-vis) spectroscopic studies were completed using a Cary 60 UV-vis spectrometer (Agilent Technologies, Santa Clara, CA, USA). EC-SERS measurements were collected using a DXR Smart Raman spectrometer equipped with a 780 nm laser (Thermo Fisher Scientific, Mississauga, ON, CA). The resolution of the spectrometer was 3 cm^{-1} and it was equipped with an air-cooled CCD detector. The DXR Smart Raman spectrometer is coupled with a Pine Research Instrumentation portable USB Wavenow potentiostat/galvanostat (Durham, NC, USA). For all control studies, the electrolyte used was 0.1M NaF solution that had been purged under argon for 30 min prior to the study being completed. For all aptamer studies, the electrolyte was a pH 7.4 phosphate buffer purged under argon for 30 min prior to the study. The applied potential ranged from 0.0V to -1.0V versus Ag/AgCl in increments of 0.1V. The Raman spectrometer used for normal Raman studies consisted of a DeltaNu (Intevac Photonics) benchtop dispersive Raman spectrometer equipped with an air-cooled CCD detector, 785 nm diode laser and an optics extension tube. The spectrometer has a resolution of 4 cm^{-1} All spectra were corrected for laser power and acquisition time for ease of data comparison. All data was analyzed using Origin 2020b Software (OriginLab Corporation Northampton, MA, USA).

3.4 Preparation of Nucleotides

3.4.1 Nucleotide base control studies

Before immobilizing aptamers on the surface of the electrode, it was important to determine what the characteristic vibrational modes were for each of the nucleotide bases. To do this, 10.0 mM nucleotide base solutions which were also 0.1M in NaF were prepared for the four nucleotide bases used in this work: adenine, guanine, cytosine and thymine. These solutions were

purged, and EC-SERS was carried out using a DXR Smart Raman spectrometer equipped with a 780 nm laser (Thermo Fisher Scientific, Mississauga, ON, CA), coupled with Pine Research Instrumentation portable USB Wavenow potentiostat/galvanostat (Durham, NC, USA).

3.4.2 Aptamer Reduction Protocol

The DNA oligomers were shipped as disulfides because the thiol functional group is not stable for an extended period of time.[64] Therefore, this disulfide had to be reduced in order to allow for preparation of the ternary self-assembled monolayer on the AgNP electrode surface. To do this, 100 μL of 1.0 M tris(2-carboxyethyl)phosphine (TCEP) hydrochloride solution (prepared fresh) was added to an Eppendorf tube that contained 1 μmol of lyophilized oligonucleotide, yielding a 10.0 mM solution of reduced oligonucleotide.[64] This solution was allowed to sit at room temperature for 2h, after which the oligonucleotide was stored in the fridge in the TCEP solution until needed.[64]

3.5 Preparation of Aptamer-Containing Ternary Monolayers for EC-SERS

Carbon screen printed electrodes were modified with nanoparticles for use in EC-SERS sensing. The screen-printed electrodes were used as received, with no pre-treatment or pre-cleaning beforehand. Three layers of the AgNP paste were drop coated onto the working electrode surface of a carbon screen printed electrode in 5 μL aliquots, drying fully between layers. Three layers of the AgNP paste is the optimal amount to ensure uniform surface coverage. Once the AgNP electrodes were prepared, the ternary (three component) SAM was assembled on the electrode surface in a sequential fashion as outlined in the next sections.

3.5.1 Immobilizing the aptamer

The AgNP electrodes were first immersed in 0.5 M KCl for 30 min, rinsed with ultrapure water and dried prior to application of the aptamer. This treatment step is done to remove citrate from the metal surface, which blocks access to the surface and is a spectral interference. The first component of the ternary SAM to be immobilized was the reduced DNA aptamer. The aptamer immobilizes onto the surface via the 5' C6 thiol linker which forms a strong Ag-S bond. The procedure for this involved drop casting 10 μL of 10 mM reduced aptamer solution onto the working electrode and allow it to dry overnight. It is important to note that removing the aptamer solution from the fridge and allowing it to warm up and redissolve was necessary, as well as drying overnight. Both factors increased the signal intensity and helped more aptamers immobilize onto the electrode surface.

3.5.2 Thiol backfilling

To block non-specific adsorption of matrix species onto areas of the substrate unoccupied by the aptamer, the AgNP electrode surface needs to be completely covered. To do this, the aptamer-modified electrode was first immersed in a solution of 5.0 mM 12-MDA in methanol for 2h, rinsed with methanol and dried. Next, the electrode was incubated in a 5.0 mM aqueous cysteamine solution for 30 min, rinsed with ultrapure water then dried. 12-MDA and cysteamine were chosen as the back-filling thiols as 12-MDA is a long chain thiol that can fill in large gaps, while cysteamine is a shorter chain thiol that is capable of filling in the smaller gaps. Further, the carboxylic acid and amine functional groups help balance the surface charge of the substrate.[48]

3.5.3 Assessment of non-specific adsorption: blocking study

Non-specific adsorption is a phenomenon that can occur wherein matrix components adsorb onto the surface of a sensor and cause interferences with the detection of the target analyte.[16] Non-specific adsorption is limited by creating a monolayer with optimized surface coverage through a process known as back-filling, as outlined above.[16] Once the ternary monolayer had been constructed for this work, it was important to test whether the blocking of non-specific adsorption was successful. Studies to test this were conducted using rhodamine 6G (R6G), which has a very strong Raman signal. Electrochemical SERS (EC-SERS) studies were conducted using a 1.0 mM R6G solution which was also 0.1 M in NaF. Both the control study and the blocking study measured the signal of R6G in solution, which simulates a matrix component trying to reach the surface from solution. First, a control study of EC-SERS for just R6G on a bare AgNP electrode was conducted. The control study was then compared to the EC-SERS signal for R6G being blocked by a 12-MDA and cysteamine monolayer that was prepared on the AgNP electrode surface.

3.5.4 Verification of aptamer persistence in the ternary monolayer

The ternary (three component) monolayer consisted of the Tro-4 aptamer modified with a C6-thiol linker on the 5' end, 12-MDA and cysteamine. All these components contain the same, or very similar Raman bands which therefore made it hard to determine if the aptamer was still immobilized to the electrode. A study was designed to verify the aptamer was still present which used deuterated thiols to back-fill the electrode surface rather than the hydrogen containing thiols. In this case, the ν(CD) modes are shifted relative to the ν(CH) modes, allowing for examination of the aptamer in the presence of both deuterated thiols. The full range grating for the DXR Smart

Raman Spectrometer (resolution is 4 cm^{-1}) was used to view the different C-H and C-D stretching vibrational modes.[65]

3.6 Testing the aptasensor with cardiac troponin I

Using the methods described above, the ternary monolayer aptasensor was prepared. The recombinant cardiac troponin I protein (>95%) that was purchased from MyBioSource (San Diego, CA, USA) was received with an initial concentration of 0.621 mg/mL of cTnI in amounts of 0.05 mg of protein per vial, ~80 μL of protein solution containing 6.0 M urea and 50 mM tris buffer pH 8. The protein was removed from the freezer, thawed and aliquoted into a separate Eppendorf tube that contained pH 7.4 phosphate buffer to obtain a cTnI solution concentration of 250 μg/mL. Next, 10 μL of the cTnI solution was drop coated onto the ternary monolayer aptasensor and allowed to dry for 1 hour. After 1 hour, the aptasensor was rinsed with Milli-Q water to remove any unbound protein. EC-SERS measurements were then obtained in a pH 7.4 phosphate buffer that was purged for 20 min. The 780 nm laser was used at 120 mW power, 60 seconds acquisition time and the high-resolution grating (resolution is 3 cm^{-1}) was used for these studies.

A control study of the protein was also conducted, where 10 μL of 250 μg/mL cTnI solution was drop coated onto a bare (non-functionalized) KCl-treated AgNP electrode and allowed to dry for 1 hour. EC-SERS measurements were then obtained in pH 7.4 phosphate that was purged with argon for 20 min.

Chapter 4: Results and Discussion

4.1 Nucleotide Base Studies

The first components analyzed for this research were the four nucleotide bases: adenine, thymine, guanine, and cytosine. It was important to determine the prominent peaks of each nucleotide base prior to building an aptasensor to determine if these bases will cause interferences with the detection of the analyte. In addition, if the Raman signal was dominated by the nucleotides, this could indicate that the aptamer is laying on the surface of the substrate, rather than immobilized as a self-assembled monolayer through the C6-SH linker. The nucleotide bases were first studied using normal Raman of the solid nucleotide powder. Electrolyte solutions containing 10.0 mM nucleotide base in 0.1M NaF were then prepared for each base for EC-SERS detection. It is important to note that while cytosine and thymine dissolved readily in Milli-Q water, both adenine and guanine required pH adjustment to dissolve. This was done by adding 1.0 mM NaOH dropwise, where adenine required 26 drops of 1.0 mM NaOH (pH ≈ 9-10) and guanine required 24 drops of 1.0 mM NaOH (pH ≈ 9-10). This was consistent with the nucleotide base studies conducted by Karaballi in 2013.[32]

4.1.1 Normal Raman

The Raman spectrometer used for normal Raman studies consisted of a DeltaNu (Intevac Photonics) benchtop dispersive Raman spectrometer equipped with an air-cooled CCD detector, 785 nm diode laser and a right-angle optics tube. The spectrometer had a resolution of 4 cm^{-1}. All spectra were corrected for laser power and acquisition time for ease of data comparison. The strong peak intensity for each nitrogen heterocycle between 600-800 cm^{-1} is characteristic of a ring breathing vibrational mode. Each base has some characteristic peaks that can be used to

distinguish these bases from each other. The ring breathing modes found between 600-800 cm^{-1} and the amide vibrations at higher wavenumbers are just a few examples: guanine (649, 1265 cm^{-1}), adenine (722, 1333 cm^{-1}) cytosine (790, 1275 cm^{-1}), and thymine (1368, 1671 cm^{-1}).[32] This can be seen in Figure 10 and the peak assignments are summarized in Tables A1-A4.

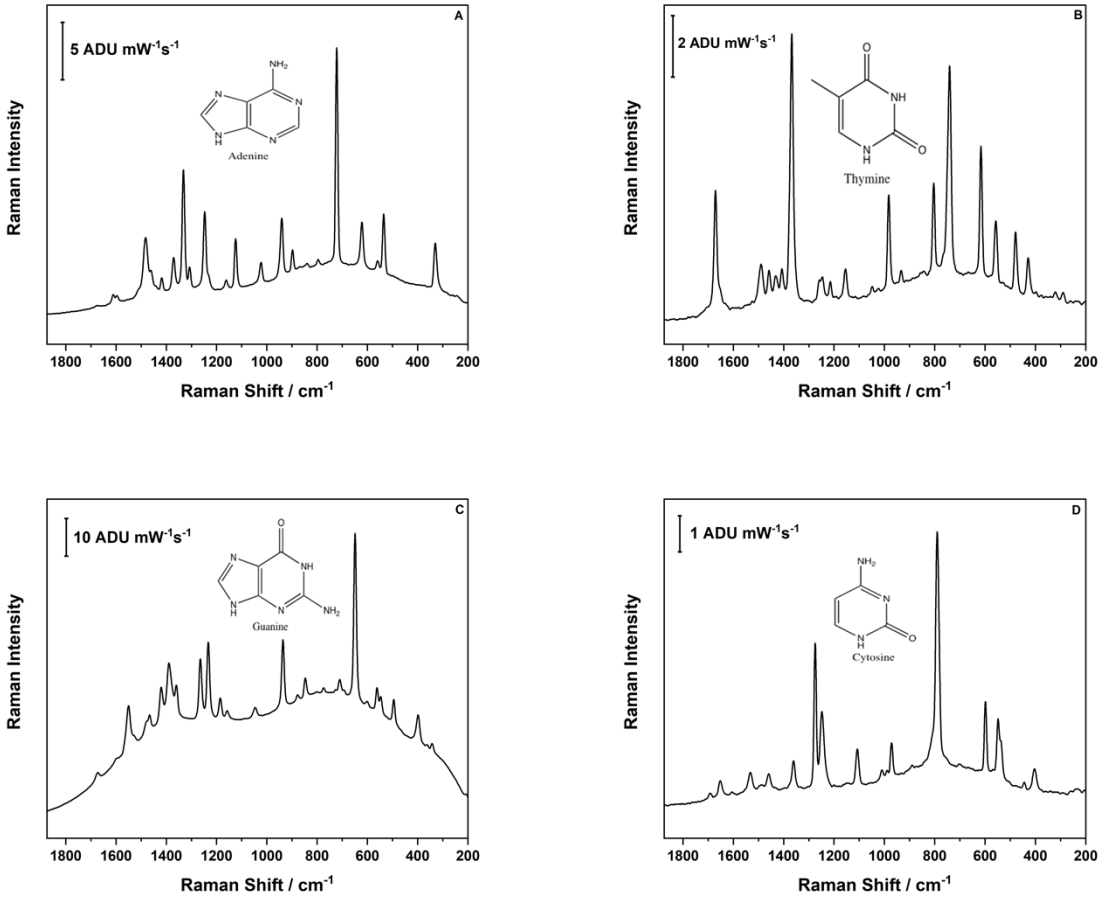

Figure 10. Normal Raman spectra of the four nucleotide base heterocycles A) Adenine B) Thymine C) Guanine D) Cytosine. Spectra were obtained by taking 10 spectra of each and averaging them. Measurements obtained using 780 nm excitation, 42.6 mW laser power and 30 s acquisition.

4.1.2 EC-SERS

Figure 11 shows a summary of the cathodic step data for each nucleotide base. It is important to note that for all bases, the intensity of signal increased significantly from open circuit potential (OCP) to more negative voltages, which is significant for two reasons. The first reason this study was important was to determine if the vibrational modes would interfere with the expected modes of cTnI. However, the more important observation is that more negative voltages pull the nucleotide base closer to the electrode surface, which could be useful when analyzing the sample for cTnI bound to the aptamer. This could indicate that as the potential is stepped in the negative potential direction, the signal of cTnI will be enhanced as it gets pulled closer to the electrode surface. Notable observations for these spectra are how the peak intensities change when in solution compared to the normal Raman spectra. For all the EC-SERS spectra, the predominant peaks were the nucleotide ring breathing modes that occur between 650 cm^{-1} and 750 cm^{-1}. Further, it is noted that the peak at 230 cm^{-1} disappears as the potential is stepped more negative. The disappearance of this peak is associated with the desorption of chloride anions from the electrode surface. The ring breathing modes for the nucleotide bases (1350 cm^{-1}) tend to increase as the electrode potential was stepped more negative corresponds to the ring breathing modes of the nucleotides and as well C-N amide stretching. This increase in intensity was determined to be due to the neutral nucleotide bases preferring the electrode surface more as the potential was stepped more negative. Overall, these findings are consistent with the findings of previous research.[32,66]

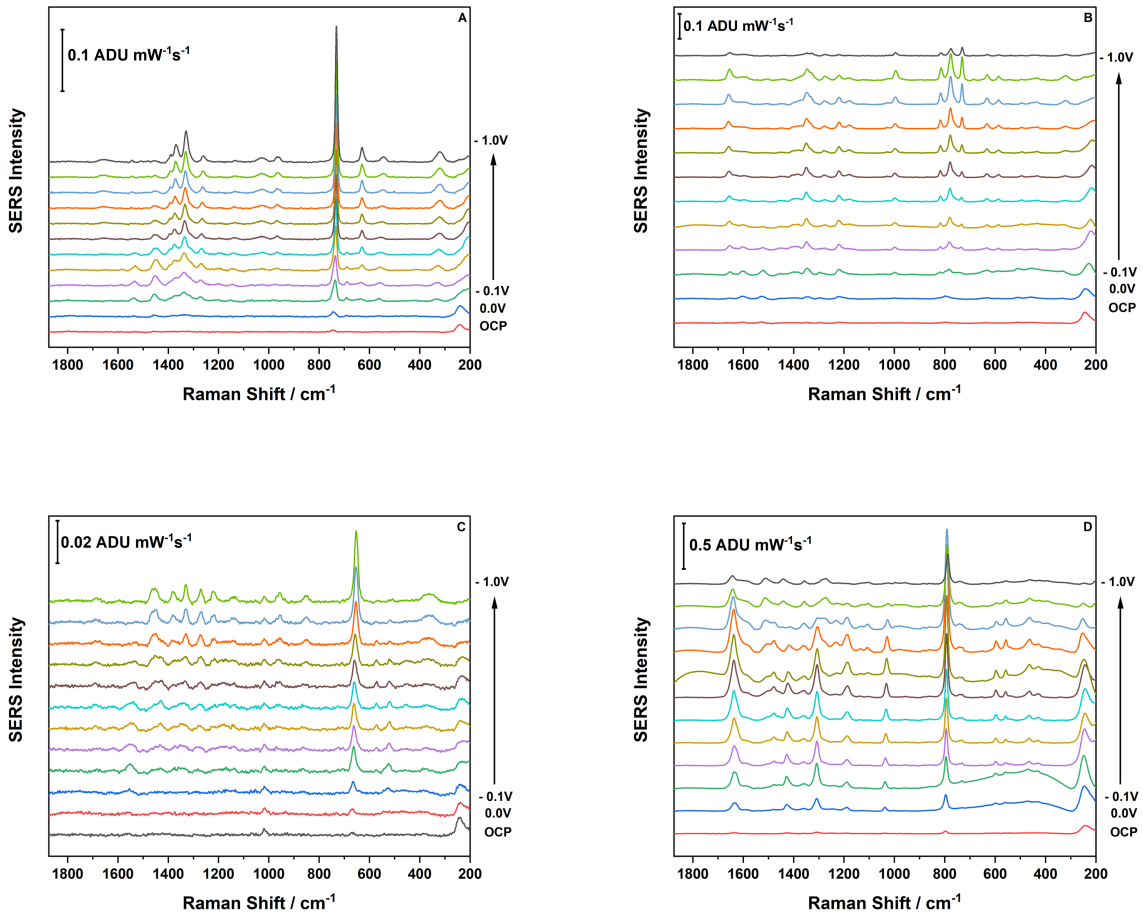

Figure 11. Depicts the EC-SERS cathodic plots of the four nucleotide base heterocycles 10.0 mM in 0.1M NaF. A) Adenine B) Thymine C) Guanine D) Cytosine. Measurements were collected using 780 nm, 80 mW power, and 30 s acquisition.

4.2 Aptamer Studies

4.2.1 EC-SERS of the Tro-4 Aptamer

A control study of the EC-SERS signal of the Tro-4 aptamer immobilized onto the electrode surface was conducted using a pH 7.4 phosphate buffer electrolyte solution. The Tro-4 aptamer modified with a C_6-SH group on the 5' end was shipped as a disulfide (S-S) since thiols oxidize spontaneously over time. Therefore, the aptamer had to be reduced to its free thiol form

prior to immobilization, which was done using tris-(2-carboxyethyl)phosphine hydrochloride (TCEP HCl), a common disulfide reducing agent.[64] Seen in Figure 12, this study showed the successful immobilization of the aptamer to the surface of the AgNP electrode. This is apparent as the Ag-S peak found at approximately 230 cm^{-1} is present for the duration of the study. It is important to note that the Ag-S peak at 230 cm^{-1} is very weak because the method of sample preparation was pipetting 10 μL of a 10.0 mM reduced aptamer solution onto the electrode surface, which means the surface coverage may not be perfect and not all "hot-spots" will have Tro-4 near them. The C-S vibrational mode at 705 cm^{-1} is present for the duration of the experiment and the peak at 1093 cm^{-1} that increases in intensity and then stays present throughout the rest of the study is characteristic of three or more straight chain carbons (trans conformation of the hydrocarbon chain), which indicates the aptamer linker becomes more ordered.[65] Peak assignments for the spectra of the Tro-4 aptamer are summarized in Table 1. The prominent peak at 1422 cm^{-1} is associated with the ring breathing modes of nucleotide bases, as well as a CH_2 scissoring vibrational mode. The Tro-4 aptamer sequence begins after the 6-carbon chain linker so it was not surprising to see the presence of nucleotides in these spectra. Further, the 6 CH_2 groups that have scissoring vibrational modes in this region could also be present. It is hypothesized that this mode is a combination of both ring breathing and CH_2 scissoring due to its broad nature. Unfortunately, no SERS reference spectra for the Tro-4 aptamer could be obtained.

Table 1. Peaks present in the Raman spectrum of the Tro-4 (C_6-SH linker) aptamer and their corresponding assignments

Peak (cm^{-1})	Assignment[65]
230	Ag-S
705	C-S
1093	C-C-C- (three or more alkyl straight chain)
1422	Nucleotide base ring breath / CH_2 scissoring
1607	Nucleotide Ring mode
2960	C-H Stretch

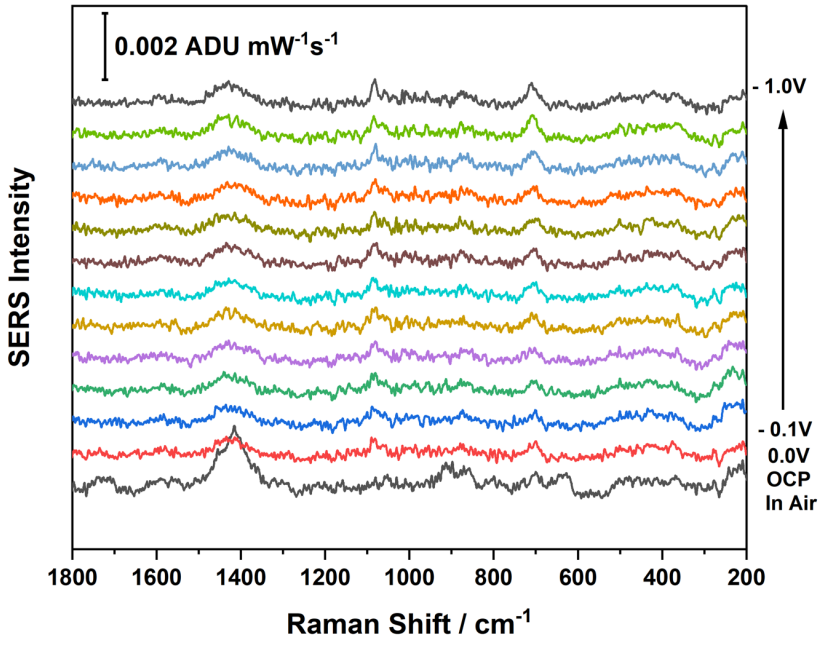

Figure 12. Cathodic step for the Tro-4 aptamer immobilized to a KCl treated AgNP electrode. Measurements were collected using 780 nm excitation, 120 mW laser power, 60 s acquisition and a pH 7.4 phosphate buffer.

4.3 Self-Assembled Monolayer (SAM) Studies and Thiol Backfilling

The SAM prepared in this work was a ternary (three component) monolayer. This ternary monolayer consists of the Tro-4 aptamer, 12-mercaptododecanoic acid (12-MDA) and cysteamine.

The 12-MDA and cysteamine were used in order to block non-specific adsorption of non-target species onto the electrode.[16,21]

4.3.1 Cysteamine

As a control study, the AgNP surface was functionalized with cysteamine by drop casting 5μL of 5.0 mM cysteamine onto the surface of a KCl-treated electrode. An electrolyte solution of pH 7.4 phosphate buffer was used for this study and the EC-SERS spectra for this study are shown in Figure 13.

This study was conducted to determine the characteristic peaks of cysteamine. It was found that the characteristic Ag-S peak at 230 cm^{-1} was present, along with C-S vibrational modes at 630 cm^{-1} (gauche) and 720 cm^{-1} (trans) and the C-C vibrations at 960 cm^{-1} and 1030 cm^{-1}.[67] As the potential was stepped more negative and then all through the anodic stepping, the peaks at 1315 cm^{-1} and 1600 cm^{-1} dominate the Raman signal. These peaks are due to phosphate anions from the buffer solution adsorbing onto the electrode, which shows the importance of preparing a uniform monolayer to limit non-specific adsorption. For this reason, the procedure for adding the cysteamine monolayer component was modified, using a previously developed procedure for thiol immobilization.[32] Peak assignments for the spectra of cysteamine are summarized in Table 2. A noteworthy observation from these spectra are the changing intensities of the gauche and trans conformations of the cysteamine, in that as the potential is stepped more negative, the trans conformation signal (720 cm^{-1}) increases while the gauche conformation signal (630 cm^{-1}) decreases. This conformational change observed indicates that as the potential is stepped more negative, the immobilized cysteamine becomes more ordered.

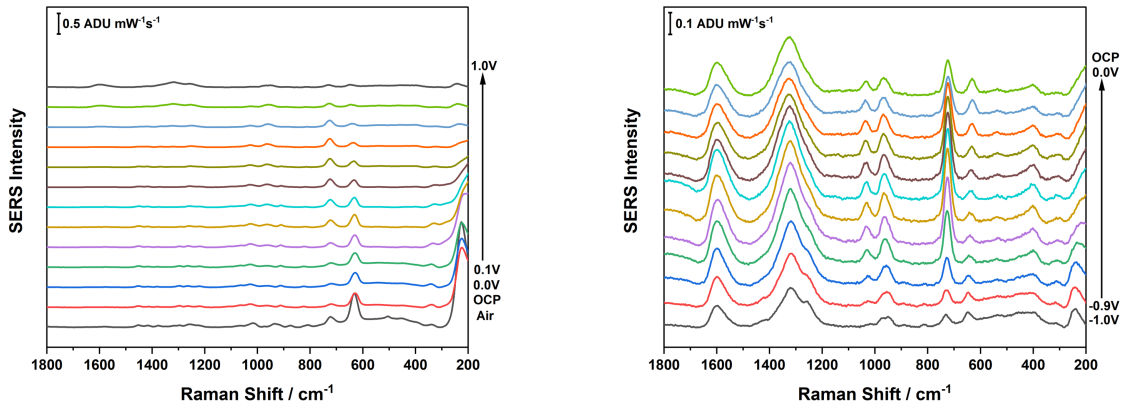

Figure 13. Cathodic (left) and anodic (right) EC-SERS spectra of cysteamine immobilized onto a KCl treated AgNP electrode. Measurments taken using a 780 nm laser, 80 mW power, 30 s acquisition time and pH 7.4 phosphate buffer electrolyte solution.

Table 2. Peaks present in the Raman spectrum of cysteamine and their corresponding assignments

Peak (cm^{-1})	**Assignment**[67]
230	Ag-S
400	-
630	C-S (gauche)
730	C-S (trans)
960	C-C(-N)
1030	C-C(-N)

4.3.2 12-MDA

Control studies were also conducted to obtain the spectra for 12-MDA. Three separate control studies were conducted for 12-MDA in order to obtain an optimal procedure for immobilizing it onto the AgNP electrode surface. The first attempt involved drop casting 10 µL of 5.0 mM 12-MDA solution onto a KCl-treated AgNP SPE, allowing it to dry and obtaining spectra using 780 nm excitation, 80mW laser power and 30s acquisition to which no 12-MDA signal was observed as seen in Figure A1. The second attempt immersed a KCl-treated AgNP electrode in 5.0 mM 12-MDA solution for 2 hours and then performed EC-SERS measurements using 780 nm excitation, 80mW laser power and 30s acquisition. Results for this second study showed some 12-

MDA signal, but the S/N was still very low as shown in Figure A2. Finally, the optimal procedure was determined to be the following: immerse a KCl-treated AgNP electrode in 5.0 mM 12-MDA solution for 2 hours and then perform EC-SERS measurements using 780 nm excitation, 120 mW laser power and 60s acquisition. Results for the optimized procedure for immobilizing 12-MDA onto the AgNP electrode surface are shown in Figure 14.

This experiment was conducted using a 0.1 M NaF electrolyte and was found to be consistent with the results of Karaballi for 12-MDA immobilized to the surface of the AgNP electrode.[32] The Ag-S peak found at approximately 230 cm^{-1} is present for the duration of the study. Furthermore, the trans C-S vibrational mode at 705 cm^{-1} is present for the duration. The peak at 1093 cm^{-1} that increases in intensity as the potential steps negative and stays present throughout the rest of the study is characteristic of the trans conformation for a hydrocarbon chain, which indicates the 12-MDA is becoming more ordered via van der Waals interactions between adjacent 12-MDA molecules.[65] Peak assignments for the spectra of 12-MDA are summarized in Table 3.

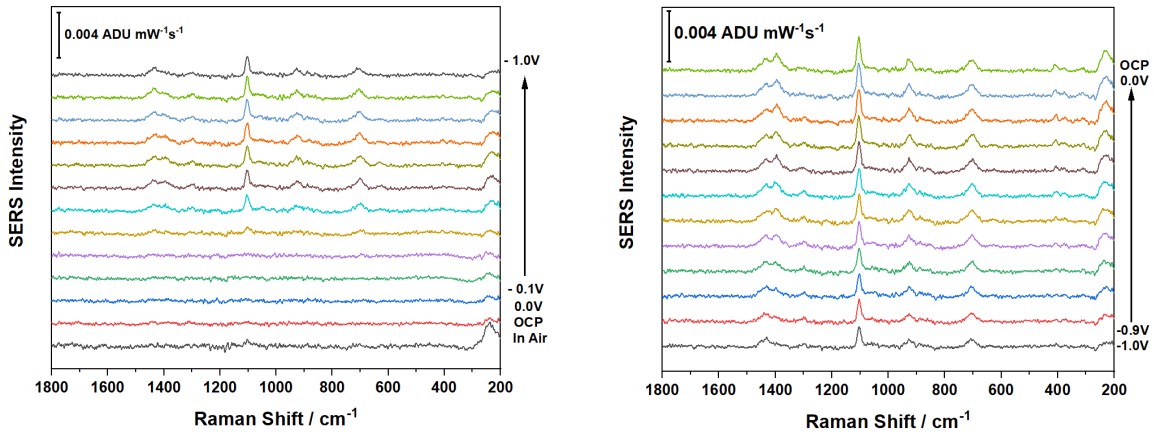

Figure 14. Cathodic (left) and anodic (right) EC-SERS plots of 12-MDA monolayer on AgNP. Collected with 120 mW power, 60 s acquisition time and 0.1 M NaF electrolyte

Table 3. Peaks present in the Raman spectrum of 12-MDA and their corresponding assignments

Peak (cm^{-1})	**Assignment**[65,67]
230	Ag-S
704	C-S (trans)
929	C-C
1100	C-C-C- (three or more alkyl straight chain)
1300	CH_2 deformation
1436	CH_2 scissoring (-CH_2COO)

4.3.3 12-MDA + Cysteamine Blocking Study

Rhodamine 6G (R6G) was used to investigate the ability of the two-component monolayer (cysteamine + 12-MDA) to block surface adsorption of non-target species. The reason R6G was chosen as a model was because it is a very strong Raman reporter due to its large Raman cross section, making it readily detectable by SERS and EC-SERS. A solution containing 1.0 mM R6G in 0.1M NaF was used for these blocking studies because if drop casted, R6G dissolves into the bulk electrolyte as can be seen in Figure A3. Figure 15 shows an overlay of the 1.0 mM R6G in 0.1M NaF control at -0.8V cathodic compared to the -0.8V cathodic spectrum of the two-component monolayer blocking 1.0 mM R6G in 0.1 M NaF. Overall, it was concluded that a monolayer consisting of both 12-MDA and cysteamine was capable of blocking >99% of the Raman signal of R6G. For comparison, the blocking efficiency for a monolayer of just 12-MDA was 93% and can be seen in Figure A4. Blocking efficiencies were calculated by comparing the peak intensity of the peak at 1314 cm^{-1} for the R6G control to the peak intensity in the blocking study. This very good blocking efficiency allowed for movement forward with confidence that the vast majority of the non-specific adsorption will be limited for the aptasensor.

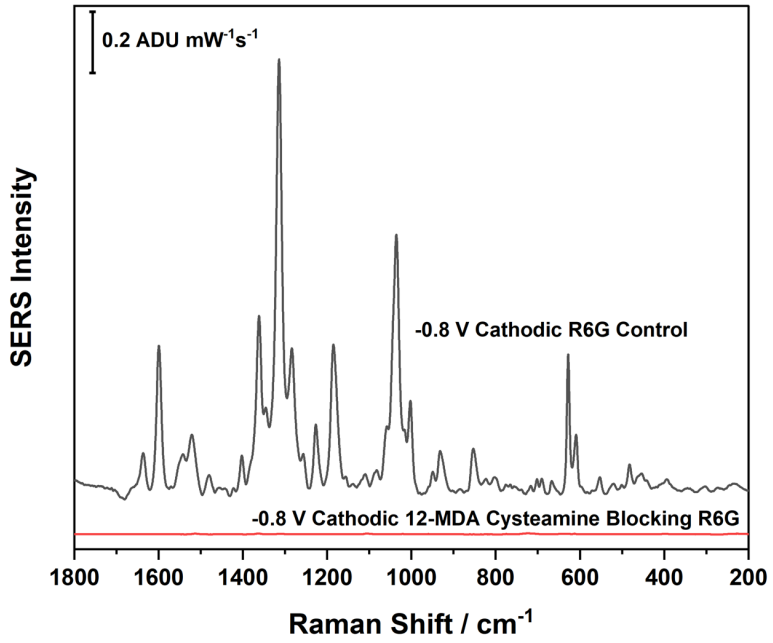

Figure 15. Overlay of (top) -0.8V cathodic stack plot of R6G control of 1 mM in 0.1 M NaF electrolyte compared to (bottom) the binary monolayer of 12-MDA and cysteamine blocking R6G 1 mM in 0.1M NaF signal

The recombinant cardiac troponin I (cTnI) from MyBioSource was shipped in a 6.0 M urea solution. Therefore, it was important to conduct a control study to determine if urea would cause any signal interference. Seen in Figure 16A is the cathodic step of a 1.0 M solution of urea in 0.1 M NaF electrolyte on a bare AgNP electrode. The prominent C-N stretch at 1000 cm^{-1} was the only main peak present for the duration of the study.[68] Figure 16B shows a monolayer of 12-MDA and cysteamine blocking the 1.0 M urea solution in 0.1 M NaF electrolyte. This spectrum shows very little interference from the urea, which allowed for the rest of the aptasensing studies to be conducted in confidence that there would be little to no non-specific adsorption occurring from the urea.

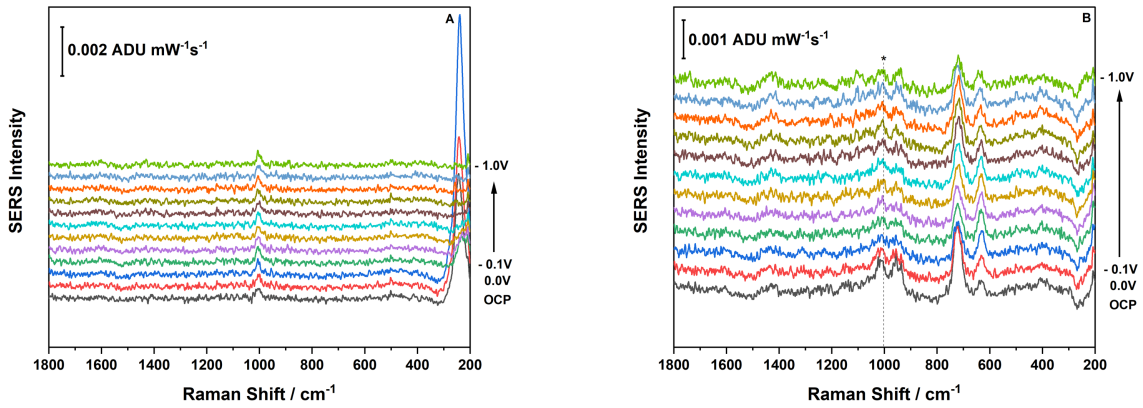

Figure 16. EC-SERS spectra of 1.0M urea in 0.1 M NaF on a bare AgNP electrode (A), compared to a monolayer of 12-MDA and cysteamine blocking 1.0 M urea in 0.1 M NaF (B). The main vibrational mode of urea is denoted in B by an asterisk. Spectra recorded with a 780 nm laser, 120 mW and 60 s acquisition.

4.3.4 Ternary Monolayer

The final steps to this project before attempting to detect cTnI was to prepare and characterize the ternary monolayer containing the Tro-4 aptamer (10 µL drop cast of 10.0 mM reduced aptamer), 12-MDA (2-hour incubation in 5.0 mM solution) and cysteamine (30 min incubation in 5.0 mM solution) in order to obtain a monolayer as shown in Figure 4. The spectra of the ternary monolayer are seen in Figure 17. The characteristic Ag-S peak found at approximately 230 cm^{-1} is present for the duration of the study. Furthermore, the trans and gauche C-S vibrational modes can be seen for the duration of the study at 705 cm^{-1} and 620 cm^{-1} respectively. Full peak assignment for the ternary monolayer of the Tro-4 aptamer, 12-MDA and cysteamine can be seen in Table 4.

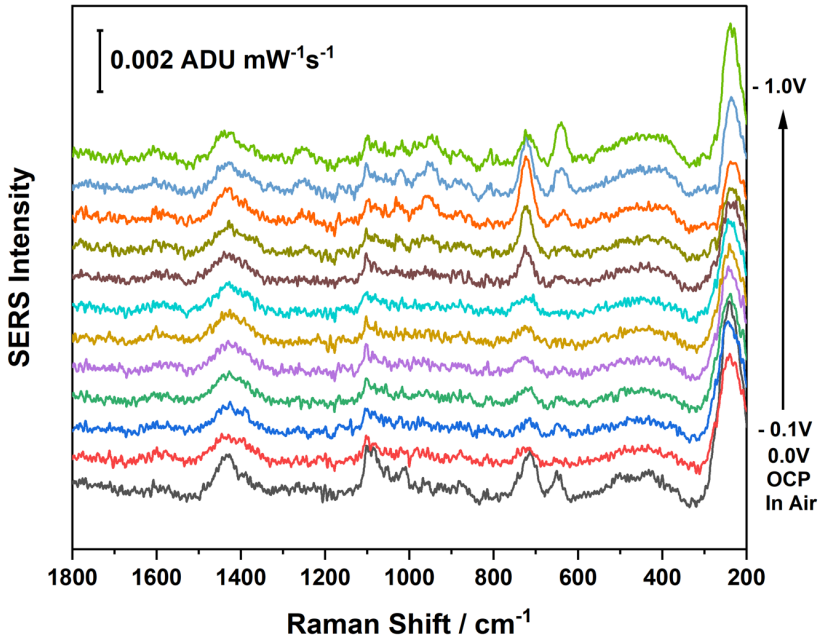

Figure 17. EC-SERS data for the cathodic step spectra for the ternary monolayer containing the Tro-4 aptamer, 12-MDA and cysteamine. The spectra were aquired using 780 nm excitation, 120 mW laser power, 60 s acquisition time and a pH 7.4 phosphate buffer electrolyte solution.

Table 4. Raman peaks present for the ternary monolayer consisting of the Tro-4 (5' C_6-SH) aptamer, 12-MDA and cysteamine.

Peak (cm^{-1})	**Assignment**[65]
230	Ag-S
669	C-S (12-MDA)
704	C-S
953	C-C(N)
1082	C-C-C- (Tro-4 three or more alkyl straight chain)
1138	C-C-C- (12-MDA three or more alkyl straight chain)
1438	Nucleotide base ring breath

A full range spectrum of just the Tro-4 aptamer immobilized onto the AgNP surface is seen in Figure 18, which was obtained so that it was possible to verify that the aptamer was still present on the surface after the ternary monolayer had been prepared. It is known that C-H and C-D

stretching modes occur at different wavenumbers, which are approximately 2900 cm^{-1} and 2100 cm^{-1} repectively.[65] Therefore, by preparing a ternary monolayer with the Tro-4 aptamer and fully deuterated thiols that were as close as possible to the backfilling thiols used in all other studies, it was possible to easily verify the aptamer was still present after monolayer preparation. Shown in Figure 19 are the overlays of both a binary (two-component) monolayer containing the Tro-4 aptamer and d_{25}-dodecane-SH, and a ternary monolayer of the Tro-4 aptamer, d_{25}-dodecane-SH and d_4-cysteamine. As seen in Figure 19, the C-H stretching mode at 2960 cm^{-1} remained present throughout the duration of these studies allowing for a simplistic comfirmation that the monolayer was assembled as expected. This study also allowed for confirmation that all monolayer components were still present. It is important to note that typically, the C-D peak displays much weaker intensity than the C-H peak, however in this specific case, it is seen that the C-D peak was stronger the the C-H peak, which occured because only 10.0 μL of a 10.0 mM aptamer solution was added to the electrode, whereas the sensor was incubated in a 5.0 mM solution of d_{25}-dodecane-SH for 2 hours and in a 5.0 mM solution of d_4-cysteamine for 30 minutes. Full peak assignments for both the binary deuterated monolayer and the ternary deuterated monolayer can be found in Tables A5-A6. All peak assignments were above the signal limit of detection, where each labelled peak was $> 3\sigma_b$.

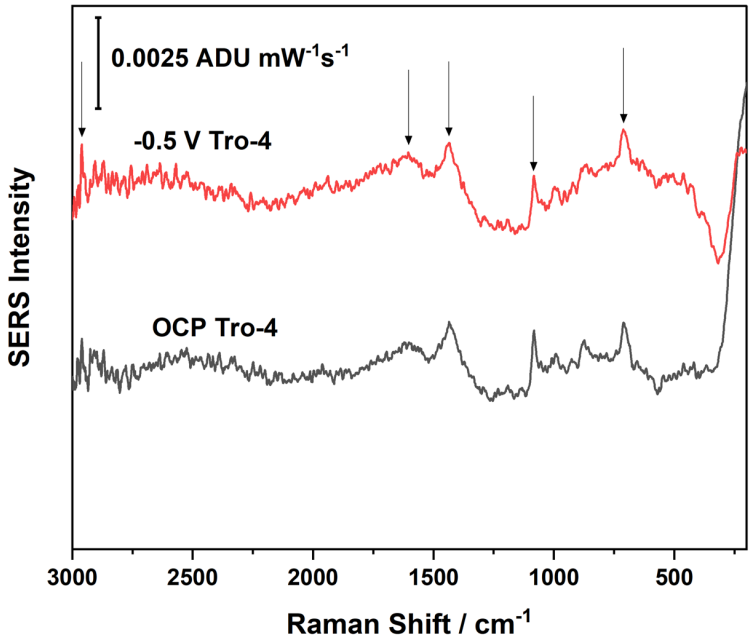

Figure 18. Overlay of the full range EC-SERS signal collected at OCP and -0.5 V for just the Tro-4 aptamer immobilized onto an AgNP electrode. Spectra were obtained using a 780 nm excitation, 120 mW laser power, 60 s acquisition time, pH 7.4 phosphate buffer and a low resolution, full range grating.

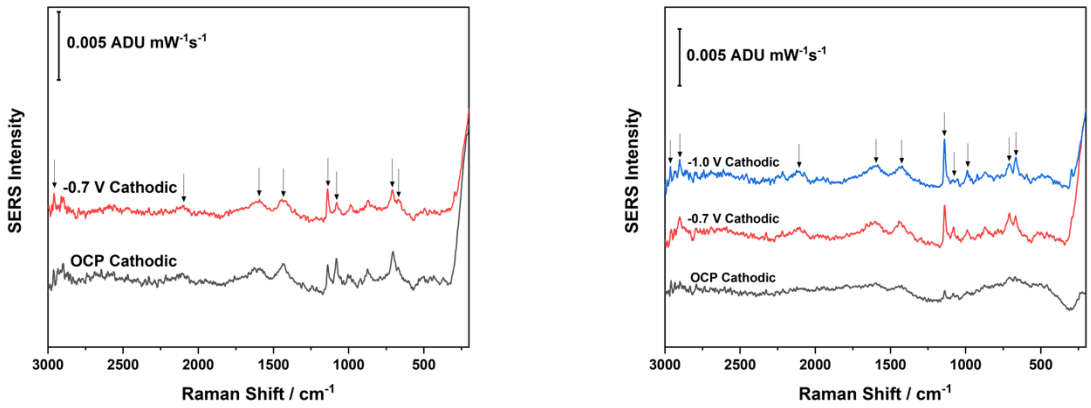

Figure 19. EC-SERS overlay plots for deuterated monolayers. The spectra on the left show cathodic overalays for a binary monolayer comprised of Tro-4 and d_{25} dodecane-SH. The spectra on the right show cathodic overlays of a ternary monolayer comprised of Tro-4, d_{25} dodecane-SH and d_4 cysteamine.

Finally, cyclic voltammograms (CVs) were plotted and compared for each component of the monolayer and are shown in Figure 20. The cyclic voltammograms provide a "picture" of the electrified interface, and can also service to inform on the state of monolayer assembly.[57] The electrochemical double layer models a parallel plate capacitor and therefore, as more layers of the monolayer are added to the electrode, the current (and related double layer capacitance) should decrease, since the effective distance between ions in solution and the electrode surface is increased.[57] This overall decrease in current as more components of the monolayer were added can be seen qualitatively in Figure 20, where the ternary monolayer displayed a much lower current in comparison to the binary monolayer of just the Tro-4 aptamer and 12-MDA.

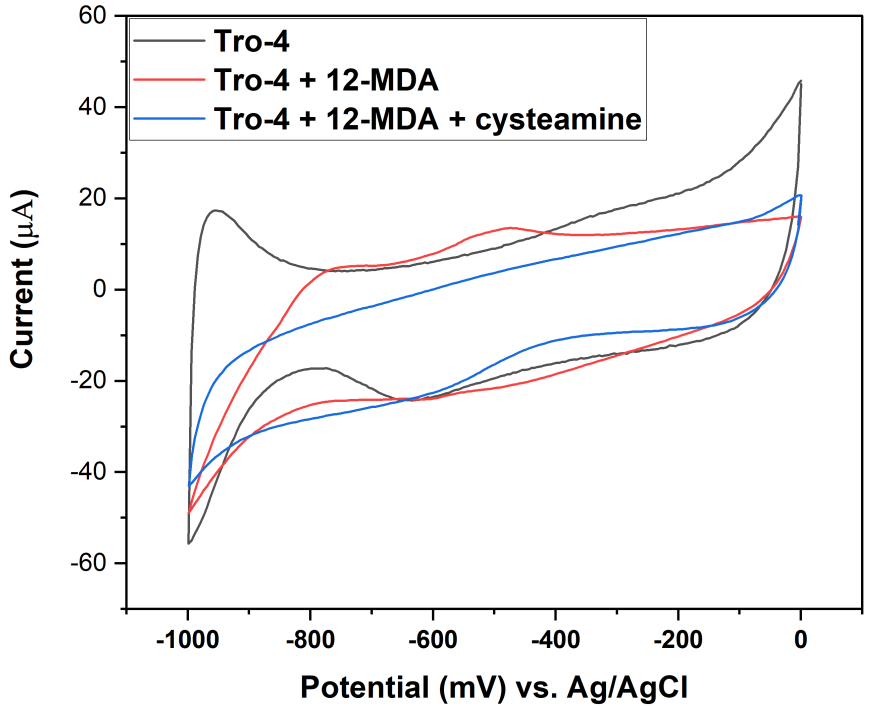

Figure 20. Shows the cyclic voltammograms of the different monolayers that were prepared. For all voltammograms, the electrolyte was a pH 7.4 phosphate buffer, 10 segments were obtained for each voltammogram at a scan rate of 50 mV/s.

4.4 Protein Studies

4.4.1 Cardiac Troponin I (cTnI)

Figure 21 shows the control study for cardiac troponin I. 10.0 μL of 250.0 μg/mL cTnI was drop coated onto a KCl-treated AgNP electrode and allowed to dry. The in-air spectrum for the control study was dominated by the signal of urea at 1000 cm^{-1}, but once the pH 7.4 phosphate buffer was added, the signal was immediately lost. Cardiac troponin I is a challenging protein to detect by SERS analysis as reported in previous works.[12] cTnI is a challenging analyte because only the aromatic amino acid residues display a strong SERS signal, and within the 210 amino acid sequence, cTnI only has 8 aromatic amino acids. Further, this study showed that on its own, it is not possible to quantitatively detect cTnI by EC-SERS, because the protein just desorbed from

the electrode surface into the bulk solution once electrolyte was added. This can be seen in Figure 21, as the expected peaks for cTnI are present in air but significantly dissipate once the pH 7.4 phosphate buffer is added

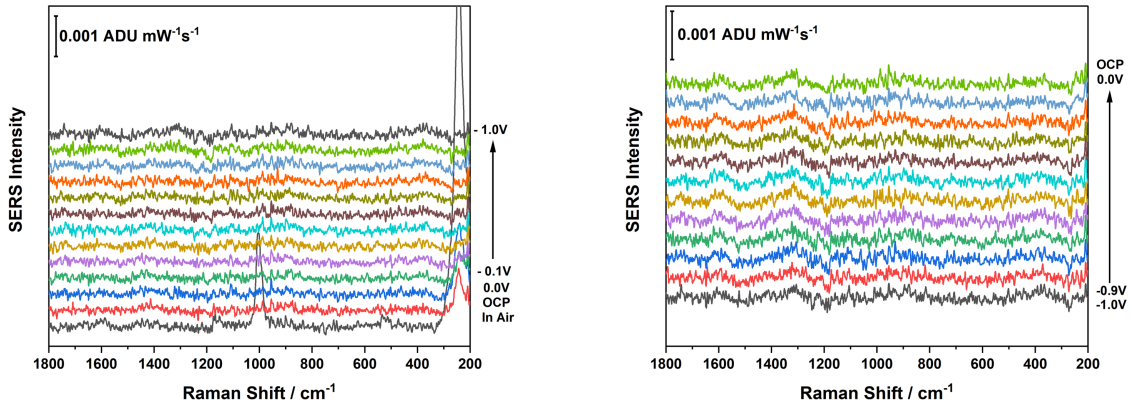

Figure 21. Cathodic (left) and anodic (right) plots of cardiac troponin I (cTnI) drop coated onto a bare KCl-treated AgNP electrode. Spectra were obtained using 780 nm laser, 120 mW power, and 60 s acquisition in pH 7.4 phosphate buffer.

Figure 22 shows the in-air spectrum of cTnI drop casted onto a bare (non-functionalized) AgNP electrode. Each individual spectrum for the cTnI control study was plotted to determine if any peaks could be seen that were characteristic of cTnI or the amino acids of tyrosine, tryptophan or phenylalanine. Viewing the in-air spectrum of cTnI, it was determined that there were some peaks present that corresponded with the aromatic amino acid residues, which further confirms the protein desorbed from the electrode surface once electrolyte was added. A summary of the peaks that were assigned with intensities above $3\sigma_b$ can be found in Table 5.

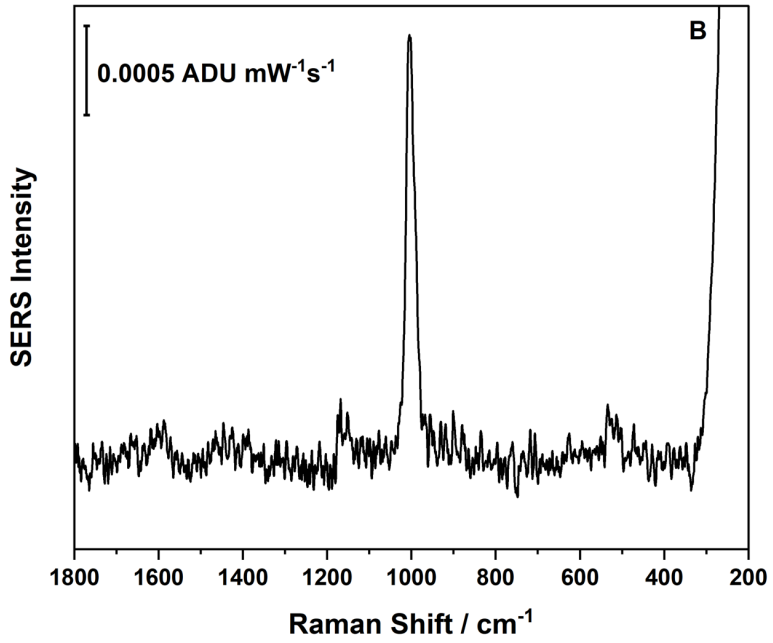

Figure 22. Shows the in-air spectrum of cardiac troponin I (cTnI) drop casted onto a bare KCl-treated AgNP electrode. Spectrum was obtained using 780 nm laser, 120 mW power, and 60 s acquisition in a pH 7.4 phosphate buffer.

Table 5. Raman peaks and corresponding assignments for cardiac troponin I (cTnI)

Peak (cm^{-1})	**Assignment**[12,65]
706	Tryptophan
720	Tryptophan
835	Tyrosine
901	Tryptophan
1078	Tryptophan / C-N stretch
1151	Tyrosine
1447	Trptophan / CH_2
1586	C=O stretch

4.5 Protein Detection Studies

4.5.1 Cardiac Troponin I (cTnI) System

The aptasensor was then tested with 10.0 μL of 250.0 μg/mL cTnI that was allowed to incubate on the sensor surface for 1 hour, followed by copious rinsing. Figure 23 shows the cathodic and anodic step plots for the study that was conducted to test the aptasensor. Upon first

glance, the spectra looked very similar, if not identical to the spectra of the ternary monolayer. Further, it was determined that none of the characteristic peaks expected for cTnI were visible when comparing these results to the literature.[12] The result of this study was not overly surprising, as SERS is a very distance-dependent technique where the analyte must be ideally within 2 nm of the plasmonic surface in order to obtain the desired enhancement.[17] A carbon-carbon bond length is approximately 0.15 nm, which means the optimum SERS enhancement distance is around 13 carbon atoms away from the surface. The aptamer used in this study contained a 6-carbon linker to immobilize the aptamer to the surface and the binding site for the protein does not occur until the 18th nucleotide residue (~0.6 nm / residue) as seen in Figure 3, meaning the protein would have been approximately 11.7 nm away from the plasmonic substrate, which is well greater than the optimal distance of SERS enhancement.

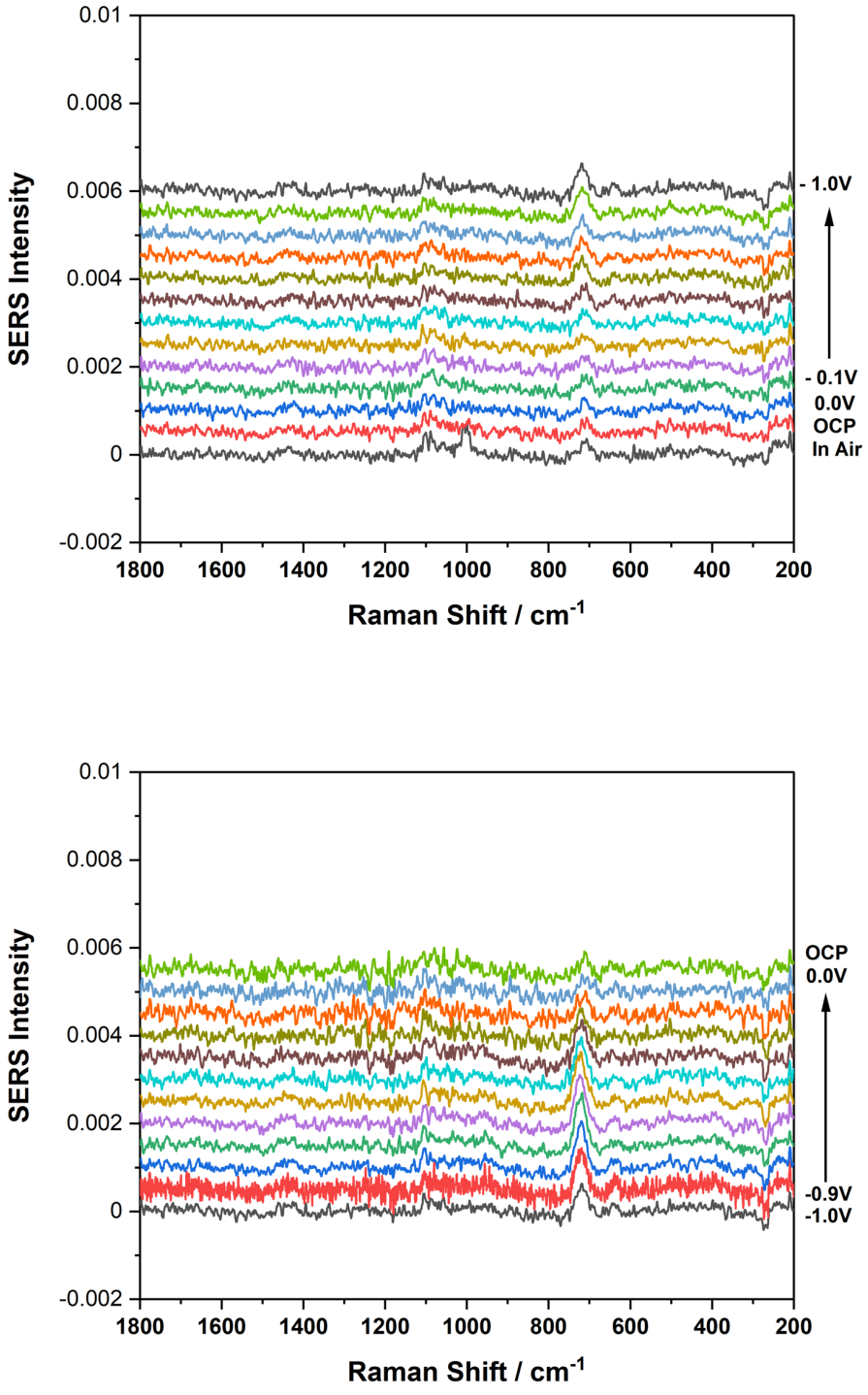

Figure 23. Cathodic (top) and anodic (bottom) plots for the aptasensor test for the detection of cTnI. Spectra were obtained using 780 nm excitation, 120 mW laser power, 60 s acquisition in a pH 7.4 phosphate buffer

Looking closer at each individual spectrum for this study and comparing it to the results of the ternary monolayer study, some differences were revealed that indicate the protein may have bound to the aptamer and caused some conformational changes to the monolayer surface. In particular, the disappearance of the Ag-S peak at 230 cm^{-1}, the C-S wavenumber shift of 20 cm^{-1}, the decreased intensity of the trans alkyl chain stretch at 1138 cm^{-1} and the disappearance of the nucleotide base ring breathing mode at 1421 cm^{-1}. The disappearance of peaks and overall changes in peak intensity indicate that when the cTnI was introduced to the system, some disorder was introduced to the monolayer, and some conformational changes occurred that causing the nucleotide base ring breathing residue to disappear. Some studies show that metal sulfur bonds can be cleaved or weakened as the potential is stepped more negative, however this is not observed in the latter ternary monolayer studies without cTnI present.[69] While it was not studied whether or not the Ag-S bond is weakened as the potential is stepping more negative, these findings indicated that the protein is causing a significant level of disorder to the monolayer, and one hypothesis for the overall changes in peak shift and intensities is that cTnI bound to the protein crowds the monolayer which in turn introduces disorder to the system.[70]

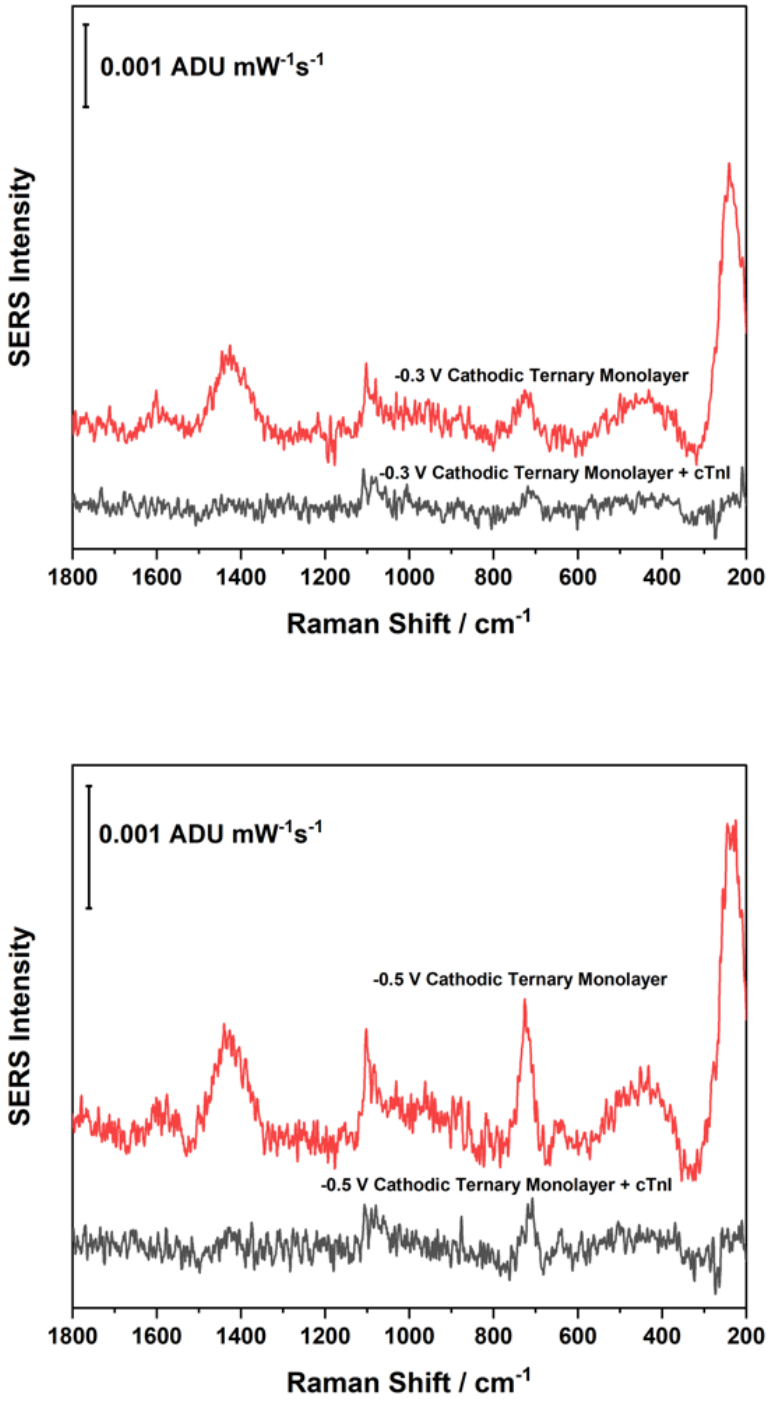

Figure 24. Stack plots comparing the ternary monolayer to the aptasensor. -0.3 V (top) and -0.5 V (bottom) were the best spectra for the aptasensor. Therefore, these were the two spectra used for comparison to the ternary monolayer control study. Spectra were obtained using a 780 nm laser, 120 mW power and 60 s acquisition time in a pH 7.4 phosphate buffer.

Chapter 5: Conclusions

This thesis work explored the development of a new aptasensor for the detection of cardiac troponin I (cTnI) using an electrochemical surface-enhanced Raman spectroscopy (EC-SERS) detection platform. First, a reduction procedure for reducing the S-S bond in the aptamer linker to SH was optimized for this project, and it was determined that 10 mM concentration of Tro-4 was the best concentration for the first component of the monolayer. After multiple attempts at developing a good ternary monolayer, it was found that 10.0 μL of 10.0 mM reduced aptamer, a two-hour incubation in 5.0 mM 12-MDA and a 30 min incubation in 5.0 mM cysteamine yielded an ideal ternary monolayer. The ideal monolayer was tested for its non-specific adsorption capabilities and was determined to block >99 % of R6G signal. The monolayer also successfully blocked the signal of urea in solution. Further, this thesis work successfully developed a method for the spectral exploration of monolayer components within an aptasensor. This method made use of the wavenumber shift that occurs when C-H bonds are exchanged for C-D bonds. This method allowed for simplistic verification that the aptamer was still immobilized to the electrode surface after all the monolayer components had been added. Studies for obtaining an EC-SERS reference spectrum of cTnI were attempted, but it was overall found that there was an issue with desorption of the protein from the plasmonic surface as soon as the electrolyte was added. Further, it was found that cTnI was not detected by this aptasensing method. However, when cTnI was introduced to the system, changes in peak intensities and wavenumbers were observed which could be an indication that when cTnI binds to the aptamer, disorder is introduced to the monolayer system due to crowding. The changes in peak intensity and wavenumber shifts indicate that protein may be bound to the aptamer, resulting in distortion of monolayer order, but is simply too far away

from the plasmonic surface to be directly detected. Overall, this thesis was able to develop new methods for monolayer verification but fell short in detecting cTnI by EC-SERS directly.

Chapter 6: Future Work

In terms of future work for this project, the main goal is to achieve quantitative detection of cTnI at clinically relevant concentrations. Further, it will be important to simulate a blood serum that contains various other matrix proteins that would be found alongside cTnI such as myoglobin, human serum albumin (HSA), hemoglobin, immunoglobulin G (IgG). Additionally, it may be found that no matter what is done, the protein is simply too far away from the SERS surface to be detected. To verify that there is an issue with distance dependence for SERS, a redox probe such as Nile Blue could be added to the electrolyte, and if the protein was complexed with the aptamer, the redox signal should be completely blocked. The issue of distance dependence can be combatted in many ways. One suggestion for overcoming distance dependence is to investigate indirect detection methods. This can be helpful when dealing with proteins because inherently there are not many strong vibrational modes found within a large protein. Another suggestion for eliminating the issue of distance dependence would be to prepare a sandwich-like substrate, by placing gold nanoparticles (AuNPs) modified with the Tro-4 aptamer on top of the existing aptasensor. Finally, other plasmonic sensing platforms could be investigated for this system, including an LSPR-based sensor which monitors refractive index changes as opposed to spectral signatures. This type of sensor may work for this system since binding of the protein to the aptamer would be expected to produce a large refractive index change which would be proportional to cTnI concentration.

Chapter 7: References

(1) Cardiovascular Diseases (CVDs). *World Health Organization*. June 11, 2021.

(2) Heart Disease in Canada. *Government of Canada*. February 10, 2017.

(3) Hasanzadeh, M.; Shadjou, N.; Eskandani, M.; de la Guardia, M.; Omidinia, E. Electrochemical Nano-Immunosensing of Effective Cardiac Biomarkers for Acute Myocardial Infarction. *TrAC Trends Anal. Chem.* **2013**, *49*, 20–30.

(4) Pourali, A.; Rashidi, M. R.; Barar, J.; Pavon-Djavid, G.; Omidi, Y. Voltammetric Biosensors for Analytical Detection of Cardiac Troponin Biomarkers in Acute Myocardial Infarction. *TrAC Trends Anal. Chem.* **2020**, 116123.

(5) Nezami, A.; Dehghani, S.; Nosrati, R.; Eskandari, N.; Taghdisi, S. M.; Karimi, G. Nanomaterial-Based Biosensors and Immunosensors for Quantitative Determination of Cardiac Troponins. *J. Pharm. Biomed. Anal.* **2018**, *159*, 425–436.

(6) Cho, E. J.; Lee, J.-W.; Ellington, A. D. Applications of Aptamers as Sensors. *Annu. Rev. Anal. Chem.* **2009**, *2*, 241–264.

(7) Tombelli, S.; Minunni, M.; Mascini, M. Analytical Applications of Aptamers. *Biosens. Bioelectron.* **2005**, *20* (12), 2424–2434.

(8) Tombelli, S.; Minunni, M.; Mascini, M. Analytical Applications of Aptamers. *Biosens. Bioelectron.* **2005**, *20* (12), 2424–2434.

(9) Munzar, J. D.; Ng, A.; Juncker, D. Duplexed Aptamers: History, Design, Theory, and Application to Biosensing. *Chem. Soc. Rev.* **2019**, *48* (5), 1390–1419.

(10) Xu, Y.; Cheng, G.; He, P.; Fang, Y. A Review: Electrochemical Aptasensors with Various Detection Strategies. *Electroanal. Int. J. Devoted Fundam. Pract. Asp. Electroanal.* **2009**, *21* (11), 1251–1259.

(11) Jo, H.; Gu, H.; Jeon, W.; Youn, H.; Her, J.; Kim, S.-K.; Lee, J.; Shin, J. H.; Ban, C. Electrochemical Aptasensor of Cardiac Troponin I for the Early Diagnosis of Acute Myocardial Infarction. *Anal. Chem.* **2015**, *87* (19), 9869–9875.

(12) Alves, R. S.; Sigoli, F. A.; Mazali, I. O. Aptasensor Based on a Flower-Shaped Silver Magnetic Nanocomposite Enables the Sensitive and Label-Free Detection of Troponin I (CTnI) by SERS. *Nanotechnology* **2020**, *31* (50), 505505.

(13) Sonntag, M. D.; Klingsporn, J. M.; Zrimsek, A. B.; Sharma, B.; Ruvuna, L. K.; Van Duyne, R. P. Molecular Plasmonics for Nanoscale Spectroscopy. *Chem. Soc. Rev.* **2014**, *43* (4), 1230–1247.

(14) Raman, C. V.; Krishnan, K. S. A New Type of Secondary Radiation. *Nature* **1928**, *121* (3048), 501–502.

(15) Pelton, M.; Aizpurua, J.; Bryant, G. Metal-nanoparticle Plasmonics. *Laser Photonics Rev.* **2008**, *2* (3), 136–159.

(16) Karaballi, R.; Nel, A.; Krishnan, S.; Blackburn, J.; Brosseau, C. Development of an Electrochemical Surface-Enhanced Raman Spectroscopy (EC-SERS) Aptasensor for Direct Detection of DNA Hybridization. *Phys. Chem. Chem. Phys.* **2015**, *17* (33), 21356–21363.

(17) Cialla, D.; März, A.; Böhme, R.; Theil, F.; Weber, K.; Schmitt, M.; Popp, J. Surface-Enhanced Raman Spectroscopy (SERS): Progress and Trends. *Anal. Bioanal. Chem.* **2012**, *403* (1), 27–54.

(18) Isaacoff, B. P.; Brown, K. A. Progress in Top-down Control of Bottom-up Assembly. *Nano Lett.* **2017**, *17* (11), 6508–6510.

(19) Farling, C. G.; Stackaruk, M. C.; Pye, C. C.; Brosseau, C. L. Fabrication of High Quality Electrochemical SERS (EC-SERS) Substrates Using Physical Vapour Deposition. *Phys. Chem. Chem. Phys.* **2021**, *23* (36), 20065–20072.

(20) Wang, Y.; Yan, B.; Chen, L. SERS Tags: Novel Optical Nanoprobes for Bioanalysis. *Chem. Rev.* **2013**, *113* (3), 1391–1428.

(21) Li, J.; Li, H.; Xu, J.; Zhao, X.; Song, S.; Zhang, H. Myocardial Infarction Biomarker C-reactive Protein Detection on Nanocomposite Aptasensor. *Biotechnol. Appl. Biochem.* **2020**.

(22) Miesfeld, R. L., , McEvoy, Megan M.,,. *Biochemistry*; 2017.

(23) Sun, X.; He, P.; Liu, S.; Ye, J.; Fang, Y. Immobilization of Single-Stranded Deoxyribonucleic Acid on Gold Electrode with Self-Assembled Aminoethanethiol Monolayer for DNA Electrochemical Sensor Applications. *Talanta* **1998**, *47* (2), 487–495.

(24) Tersch, C.; Lisdat, F. Label-Free Detection of Protein–DNA Interactions Using Electrochemical Impedance Spectroscopy. *Electrochimica Acta* **2011**, *56* (22), 7673–7679.

(25) Robertson, D. L.; Joyce, G. F. Selection in Vitro of an RNA Enzyme That Specifically Cleaves Single-Stranded DNA. *Nature* **1990**, *344* (6265), 467–468.

(26) Ellington, A. D.; Szostak, J. W. In Vitro Selection of RNA Molecules That Bind Specific Ligands. *nature* **1990**, *346* (6287), 818–822.

(27) Tuerk, C.; Gold, L. Systematic Evolution of Ligands by Exponential Enrichment: RNA Ligands to Bacteriophage T4 DNA Polymerase. *science* **1990**, *249* (4968), 505–510.

(28) Villalonga, A.; Estabiel, I.; Pérez-Calabuig, A. M.; Mayol, B.; Parrado, C.; Villalonga, R. Amperometric Aptasensor with Sandwich-Type Architecture for Troponin I Based on

Carboxyethylsilanetriol-Modified Graphene Oxide Coated Electrodes. *Biosens. Bioelectron.* **2021**, *183*, 113203.

(29) Iliuk, A. B.; Hu, L.; Tao, W. A. Aptamer in Bioanalytical Applications. *Anal. Chem.* **2011**, *83* (12), 4440–4452.

(30) McConnell, E. M.; Cozma, I.; Morrison, D.; Li, Y. Biosensors Made of Synthetic Functional Nucleic Acids toward Better Human Health. *Anal. Chem.* **2019**, *92* (1), 327–344.

(31) Velasco-Garcia, M.; Missailidis, S. New Trends in Aptamer-Based Electrochemical Biosensors. *Gene Ther. Mol. Biol.* **2009**, *13* (1), 1–10.

(32) Karaballi, R. A. Development of a DNA-Based Aptasensor for Rapid Detection of Tuberculosis. **2013**.

(33) Zhang, H.; Ma, X.; Liu, Y.; Duan, N.; Wu, S.; Wang, Z.; Xu, B. Gold Nanoparticles Enhanced SERS Aptasensor for the Simultaneous Detection of Salmonella Typhimurium and Staphylococcus Aureus. *Biosens. Bioelectron.* **2015**, *74*, 872–877.

(34) Wang, Z.; Zong, S.; Wang, Y.; Li, N.; Li, L.; Lu, J.; Wang, Z.; Chen, B.; Cui, Y. Screening and Multiple Detection of Cancer Exosomes Using an SERS-Based Method. *Nanoscale* **2018**, *10* (19), 9053–9062.

(35) Tang, L.; Li, S.; Han, F.; Liu, L.; Xu, L.; Ma, W.; Kuang, H.; Li, A.; Wang, L.; Xu, C. SERS-Active Au@ Ag Nanorod Dimers for Ultrasensitive Dopamine Detection. *Biosens. Bioelectron.* **2015**, *71*, 7–12.

(36) Yoon, J.; Choi, N.; Ko, J.; Kim, K.; Lee, S.; Choo, J. Highly Sensitive Detection of Thrombin Using SERS-Based Magnetic Aptasensors. *Biosens. Bioelectron.* **2013**, *47*, 62–67.

(37) Li, C.; Fan, P.; Liang, A.; Jiang, Z. Using Ca-Doped Carbon Dots as Catalyst to Amplify Signal to Determine Ultratrace Thrombin by Free-Label Aptamer-SERS Method. *Mater. Sci. Eng. C* **2019**, *99*, 1399–1406.

(38) Jiang, N.; Zhu, T.; Hu, Y. Competitive Aptasensor with Gold Nanoparticle Dimers and Magnetite Nanoparticles for SERS-Based Determination of Thrombin. *Microchim. Acta* **2019**, *186* (12), 1–8.

(39) Sharma, B.; Frontiera, R. R.; Henry, A.-I.; Ringe, E.; Van Duyne, R. P. SERS: Materials, Applications, and the Future. *Mater. Today* **2012**, *15* (1–2), 16–25.

(40) Li, M. X.; Hwang, P. M. Structure and Function of Cardiac Troponin C (TNNC1): Implications for Heart Failure, Cardiomyopathies, and Troponin Modulating Drugs. *Gene* **2015**, *571* (2), 153–166.

(41) Negahdary, M. Aptamers in Nanostructure-Based Electrochemical Biosensors for Cardiac Biomarkers and Cancer Biomarkers: A Review. *Biosens. Bioelectron.* **2020**, *152*, 112018.

(42) Katrukha, I. Human Cardiac Troponin Complex. Structure and Functions. *Biochem. Mosc.* **2013**, *78* (13), 1447–1465.

(43) Li, M. X.; Hwang, P. M. Structure and Function of Cardiac Troponin C (TNNC1): Implications for Heart Failure, Cardiomyopathies, and Troponin Modulating Drugs. *Gene* **2015**, *571* (2), 153–166.

(44) Schlücker, S. Surface-Enhanced Raman Spectroscopy: Concepts and Chemical Applications. *Angew. Chem. Int. Ed.* **2014**, *53* (19), 4756–4795.

(45) Harris, D. C.; Bertolucci, M. D. *Symmetry and Spectroscopy: An Introduction to Vibrational and Electronic Spectroscopy*; Courier Corporation, 1989.

(46) Kudelski, A. Analytical Applications of Raman Spectroscopy. *Talanta* **2008**, *76* (1), 1–8.

(47) Doering, W. E.; Piotti, M. E.; Natan, M. J.; Freeman, R. G. SERS as a Foundation for Nanoscale, Optically Detected Biological Labels. *Adv. Mater.* **2007**, *19* (20), 3100–3108.

(48) Wang, Z.; Zong, S.; Wu, L.; Zhu, D.; Cui, Y. SERS-Activated Platforms for Immunoassay: Probes, Encoding Methods, and Applications. *Chem. Rev.* **2017**, *117* (12), 7910–7963.

(49) Movasaghi, Z.; Rehman, S.; Rehman, I. U. Raman Spectroscopy of Biological Tissues. *Appl. Spectrosc. Rev.* **2007**, *42* (5), 493–541.

(50) Bantz, K. C.; Meyer, A. F.; Wittenberg, N. J.; Im, H.; Kurtuluş, Ö.; Lee, S. H.; Lindquist, N. C.; Oh, S.-H.; Haynes, C. L. Recent Progress in SERS Biosensing. *Phys. Chem. Chem. Phys.* **2011**, *13* (24), 11551–11567.

(51) Jeanmaire, D. L.; Van Duyne, R. P. Surface Raman Spectroelectrochemistry: Part I. Heterocyclic, Aromatic, and Aliphatic Amines Adsorbed on the Anodized Silver Electrode. *J. Electroanal. Chem. Interfacial Electrochem.* **1977**, *84* (1), 1–20.

(52) Albrecht, M. G.; Creighton, J. A. Anomalously Intense Raman Spectra of Pyridine at a Silver Electrode. *J. Am. Chem. Soc.* **1977**, *99* (15), 5215–5217.

(53) Lane, L. A.; Qian, X.; Nie, S. SERS Nanoparticles in Medicine: From Label-Free Detection to Spectroscopic Tagging. *Chem. Rev.* **2015**, *115* (19), 10489–10529.

(54) Porter, M. D.; Lipert, R. J.; Siperko, L. M.; Wang, G.; Narayanan, R. SERS as a Bioassay Platform: Fundamentals, Design, and Applications. *Chem. Soc. Rev.* **2008**, *37* (5), 1001–1011.

(55) Rycenga, M.; Cobley, C. M.; Zeng, J.; Li, W.; Moran, C. H.; Zhang, Q.; Qin, D.; Xia, Y. Controlling the Synthesis and Assembly of Silver Nanostructures for Plasmonic Applications. *Chem. Rev.* **2011**, *111* (6), 3669–3712.

(56) Margenau, H. Van Der Waals Forces. *Rev. Mod. Phys.* **1939**, *11* (1), 1.

(57) Wang, J. *Analytical Electrochemistry*, 2nd ed.; Wiley-VCH: New York, 2000.

(58) Grahame, D. C. The Electrical Double Layer and the Theory of Electrocapillarity. *Chem. Rev.* **1947**, *41* (3), 441–501.

(59) Wain, A. J.; O'Connell, M. A. Advances in Surface-Enhanced Vibrational Spectroscopy at Electrochemical Interfaces. *Adv. Phys. X* **2017**, *2* (1), 188–209.

(60) Eisnor, M.; McLeod, K.; Bindesri, S.; Svoboda, S.; Wustholz, K.; Brosseau, C. L. Electrochemical Surface-Enhanced Raman Spectroscopy (EC-SERS): A Tool for the Identification of Polyphenolic Components in Natural Lake Pigments. *Phys. Chem. Chem. Phys.* **2021**.

(61) Wu, D.-Y.; Li, J.-F.; Ren, B.; Tian, Z.-Q. Electrochemical Surface-Enhanced Raman Spectroscopy of Nanostructures. *Chem. Soc. Rev.* **2008**, *37* (5), 1025–1041.

(62) Greene, B.; Alhatab, D.; Pye, C.; Brosseau, C. Electrochemical-Surface Enhanced Raman Spectroscopic (EC-SERS) Study of 6-Thiouric Acid: A Metabolite of the Chemotherapy Drug Azathioprine. *J. Phys. Chem. C* **2017**, *121* (14), 8084–8090.

(63) Lee, P.; Meisel, D. Adsorption and Surface-Enhanced Raman of Dyes on Silver and Gold Sols. *J. Phys. Chem.* **1982**, *86* (17), 3391–3395.

(64) Reduction for Oligonucleotides with Thiol Modifications, 2020.

(65) Socrates, G. *Infrared and Raman Characteristic Group Frequencies: Tables and Charts*; John Wiley & Sons LTD, 2001.

(66) Lynk, T. P.; Sit, C. S.; Brosseau, C. L. Electrochemical Surface-Enhanced Raman Spectroscopy as a Platform for Bacterial Detection and Identification. *Anal. Chem.* **2018**, *90* (21), 12639–12646.

(67) Kudelski, A.; Hill, W. Raman Study on the Structure of Cysteamine Monolayers on Silver. *Langmuir* **1999**, *15* (9), 3162–3168.

(68) Keuleers, R.; Desseyn, H.; Rousseau, B.; Van Alsenoy, C. Vibrational Analysis of Urea. *J. Phys. Chem. A* **1999**, *103* (24), 4621–4630.

(69) Inagaki, M.; Motobayashi, K.; Ikeda, K. Electrochemical THz-SERS Observation of Thiol Monolayers on Au (111) and (100) Using Nanoparticle-Assisted Gap-Mode Plasmon Excitation. *J. Phys. Chem. Lett.* **2017**, *8* (17), 4236–4240.

(70) Rozenblum, G. T.; Pollitzer, I. G.; Radrizzani, M. Challenges in Electrochemical Aptasensors and Current Sensing Architectures Using Flat Gold Surfaces. *Chemosensors* **2019**, *7* (4), 57.

(71) Zhang, L.; Li, Q.; Tao, W.; Yu, B.; Du, Y. Quantitative Analysis of Thymine with Surface-Enhanced Raman Spectroscopy and Partial Least Squares (PLS) Regression. *Anal. Bioanal. Chem.* **2010**, *398* (4), 1827–1832.

(72) Yu, L.-J.; Pang, R.; Tao, S.; Yang, H.-T.; Wu, D.-Y.; Tian, Z.-Q. Solvent Effect and Hydrogen Bond Interaction on Tautomerism, Vibrational Frequencies, and Raman Spectra of Guanine: A Density Functional Theoretical Study. *J. Phys. Chem. A* **2013**, *117* (20), 4286–4296.

(73) Billinghurst, B. E.; Loppnow, G. R. Excited-State Structural Dynamics of Cytosine from Resonance Raman Spectroscopy. *J. Phys. Chem. A* **2006**, *110* (7), 2353–2359.

Chapter 8: Appendix

Table A1. Peaks present in the Raman spectrum of adenine and their corresponding assignments

Peak (cm^{-1})	**Assignment**[65]
331	-
535	C-H and NH wagging
623	C-C twist
722	Adenine ring breathing
897	-
942	Ring deformation
1024	NH_2 rocking
1124	C-N
1249	-
1333	H-bending & Ring stretch
1372	Adenine ring breathing
1420	Adenine ring breathing
1483	Adenine ring breathing

Table A2. Peaks present in the Raman spectrum of Thymine and their corresponding assignments

Peak (cm^{-1})	**Assignment**[65,71]
428	-
479	DNA
558	-
617	N-H wagging
740	Ring breath & N-H wagging
803	C-H wagging
933	-
983	Ring breath & CH_3 asymmetric stretch
1155	-
1216	C-N stretching
1251	C-N stretching, Thymine ring breath, Amide III
1368	Thymine ring breathing
1409	-
1433	-
1460	CH_3 deformation
1491	C-N
1671	Amide I

Table A3. Peaks present in the Raman spectrum of Guanine and their corresponding assignments

Peak (cm^{-1})	**Assignment**[65,72]
400	-
494	N-H bend
561	NH_2 wagging
649	Guanine ring breathing mode
938	C-C stretch
1047	-
1161	C-N stretch
1186	-
1233	Amide III
1265	Amide III
1360	N-H bend, C-N stretch
1390	NH_2 rocking and C-H rocking
1421	Guanine ring breath
1468	C=N
1479	Amide II
1551	Amide II
1671	Amide I

Table A4. Peaks present in the Raman spectrum of cytosine and their corresponding assignments

Peak (cm^{-1})	**Assignment**[65,73]
401	-
550	C-N torsion
600	C-N torsion
790	Cytosine ring breathing mode & C=O deformation
971	C-C wagging
989	-
1010	-
1108	C-N stretch
1247	NH_2 cytosine rocking
1275	Amide II
1362	C-N stretch
1461	-
1532	Amide carbonyl, Amide III
1652	Amide I
1693	-

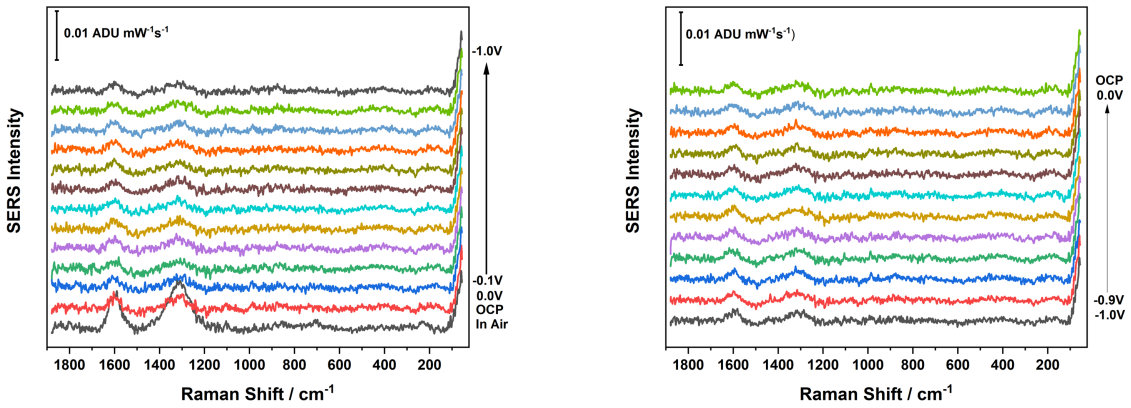

Figure A1. Cathodic step (left) and anodic step (right) of 10.0 µL of 5.0 M MDA drop casted onto a AgNP KCl-treated electrode. Spectra were acquired using 780 nm excitation, 80 mW laser power, 30 s acquisition and a pH 7.4 phosphate buffer.

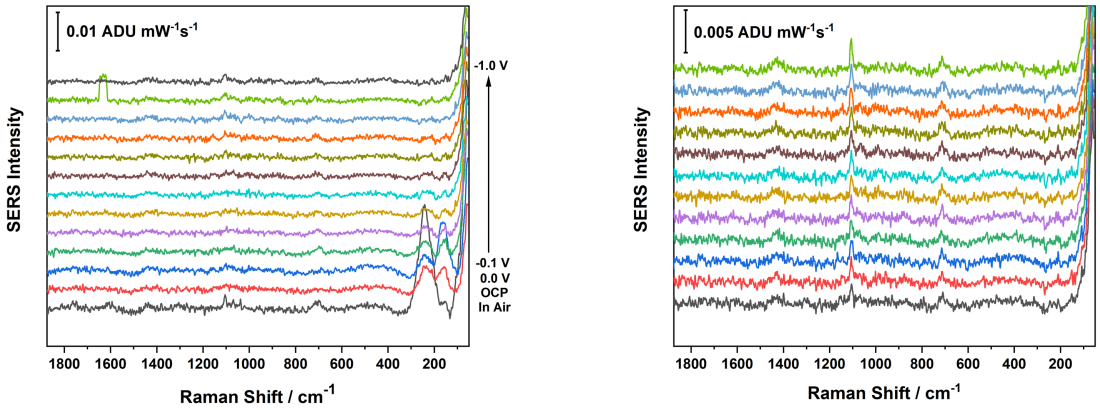

Figure A2. Cathodic step (left) and anodic step (right) of a 12-MDA functionalized AgNP electrode (0.5 M KCl-treatment for 30 min then, a 2-hour incubation in 5.0 M MDA). Spectra were acquired using 780 nm excitation, 80 mW laser power, 30 s acquisition and a pH 7.4 phosphate buffer.

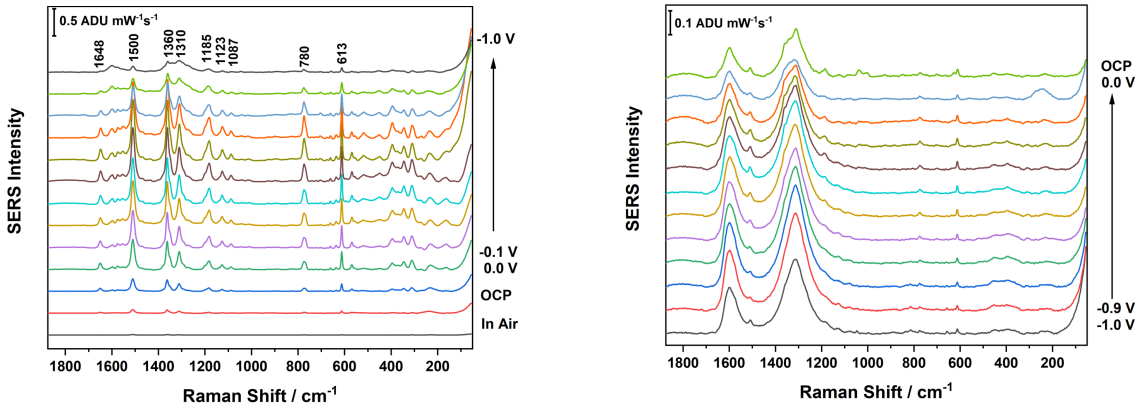

Figure A3. Cathodic step (left) and anodic step (right) of 10.0 µL of 1.0 M R6G drop casted onto a KCl-treated AgNP electrode. Spectra were acquired using 780 nm excitation, 80 mW laser power, 30 s acquisition and a pH 7.4 phosphate buffer.

Table A5. Raman peaks present and corresponding assignments for the binary monolayer containing the Tro-4 (5' C_6-SH) aptamer and d_{25}-dodecane-SH.

Peak (cm^{-1})	**Assignment**[65]
230	Ag-S
669	C-S (d_{25}-dodecane-SH)
704	C-S
1082	C-C-C- (Tro-4 three or more alkyl straight chain)
1138	C-C-C- (d_{25}-dodec. three or more alkyl straight chain)
1438	Nucleotide base ring breath
1607	Nucleotide base Ring stretch
2097	C-D stretch
2960	C-H Stretch

Table A6. Raman peaks present and corresponding assignments for the ternary monolayer containing the Tro-4 (5' C_6-SH) aptamer, d_{25}-dodecane-SH and d_4 cysteamine

Peak (cm^{-1})	**Assignment**[65]
230	Ag-S
669	C-S (d_{25}-dodecane-SH)
704	C-S
953	C-C(N)
1082	C-C-C- (Tro-4 three or more alkyl straight chain)

1138	C-C-C- (d_{25}-dodec. three or more alkyl straight chain)
1438	Nucleotide base ring breath
1607	Nucleotide base Ring stretch
2097	C-D stretch
2960	C-H Stretch

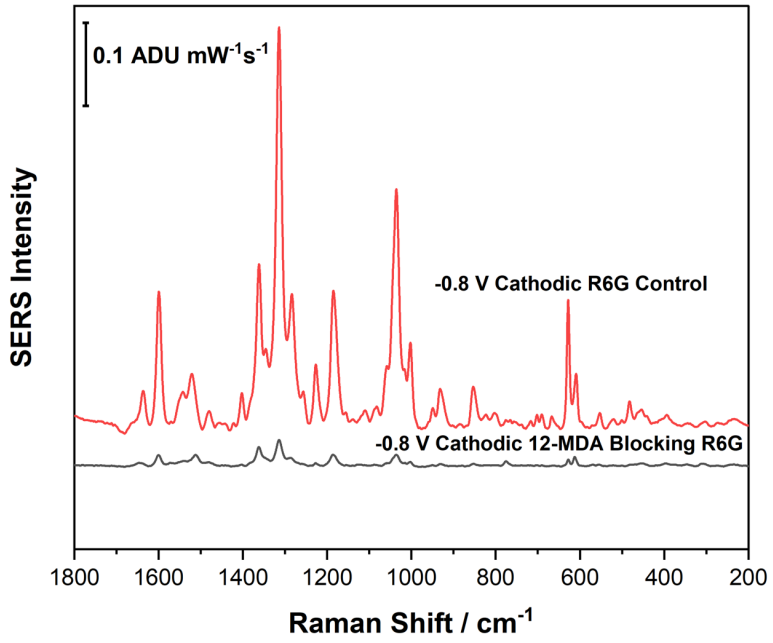

Figure A4. -0.8V cathodic overlay plot of R6G control 1mM in 0.1 M NaF electrolyte compared to of the monolayer of 12-MDA blocking R6G 1mM in 0.1 M NaF signal

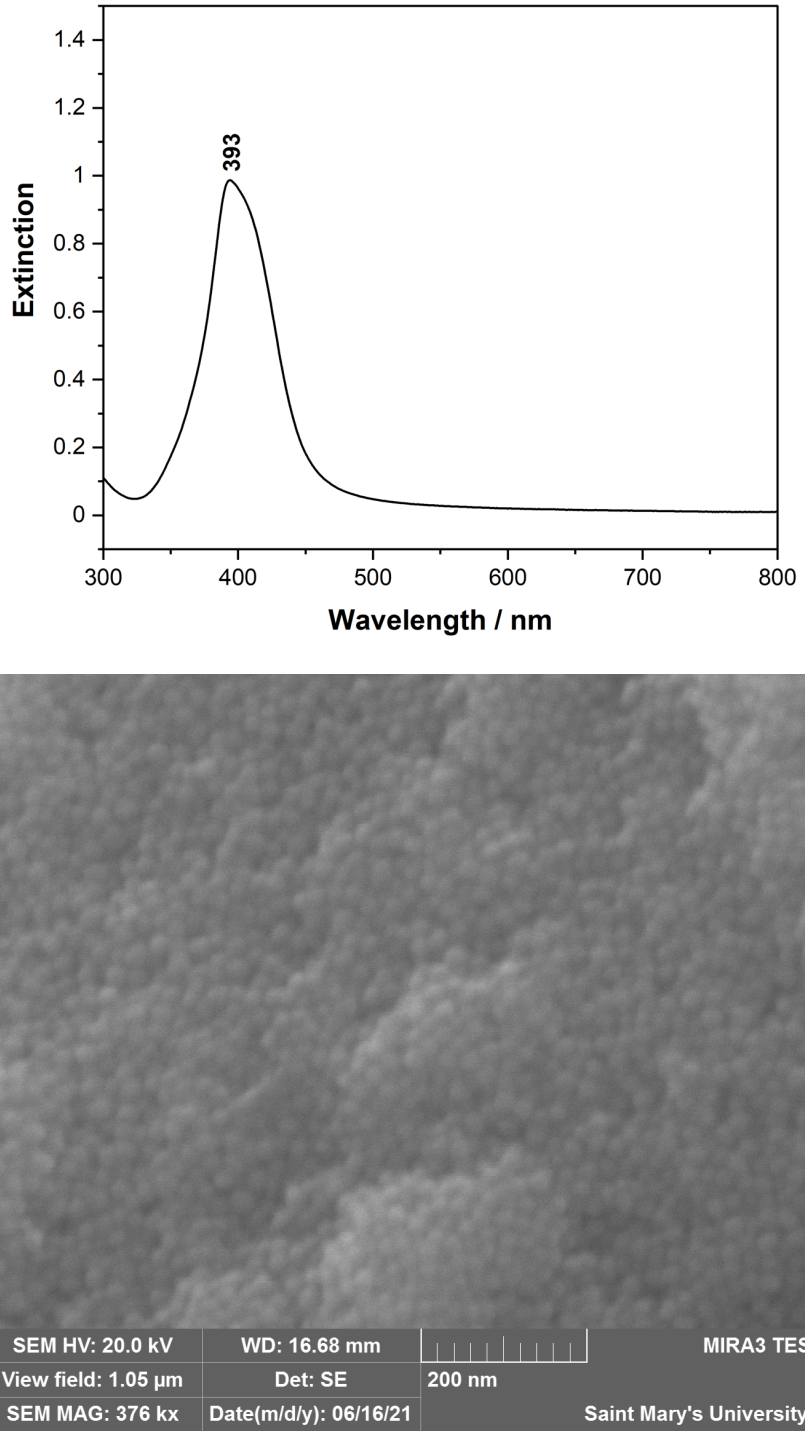

Figure A5. UV-Vis spectrum (top) and SEM image of AgNP (bottom) used for characterization

Electrochemical Aptasensor of Cardiac Troponin I for the Early Diagnosis of Acute Myocardial Infarction

Author: Hunho Jo, Hyunwoo Gu, Weejeong Jeon, et al

Publication: Analytical Chemistry

Publisher: American Chemical Society

Date: Oct 1, 2015

PERMISSION/LICENSE IS GRANTED FOR YOUR ORDER AT NO CHARGE

This type of permission/license, instead of the standard Terms and Conditions, is sent to you because no fee is being charged for your order. Please note the following:

- Permission is granted for your request in both print and electronic formats, and translations.
- If figures and/or tables were requested, they may be adapted or used in part.
- Please print this page for your records and send a copy of it to your publisher/graduate school.
- Appropriate credit for the requested material should be given as follows: "Reprinted (adapted) with permission from {COMPLETE REFERENCE CITATION}. Copyright {YEAR} American Chemical Society." Insert appropriate information in place of the capitalized words.
- One-time permission is granted only for the use specified in your RightsLink request. No additional uses are granted (such as derivative works or other editions). For any uses, please submit a new request.

If credit is given to another source for the material you requested from RightsLink, permission must be obtained from that source.

BACK CLOSE WINDOW

Analytical applications of aptamers

Author: S. Tombelli,M. Minunni,M. Mascini

Publication: Biosensors and Bioelectronics

Publisher: Elsevier

Date: 15 June 2005

Order Completed

Thank you for your order.

This Agreement between Sam Julien ("You") and Elsevier ("Elsevier") consists of your license details and the terms and conditions provided by Elsevier and Copyright Clearance Center.

Your confirmation email will contain your order number for future reference.

Printable Details

License Number	5257331425946
License date	Feb 27, 2022

Licensed Content

Licensed Content Publisher	Elsevier
Licensed Content Publication	Biosensors and Bioelectronics
Licensed Content Title	Analytical applications of aptamers
Licensed Content Author	S. Tombelli,M. Minunni,M. Mascini
Licensed Content Date	Jun 15, 2005
Licensed Content Volume	20
Licensed Content Issue	12
Licensed Content Pages	11

Order Details

Type of Use	reuse in a thesis/dissertation
Portion	figures/tables/illustrations
Number of figures/tables/illustrations	1
Format	electronic
Are you the author of this Elsevier article?	No
Will you be translating?	No

Structure and function of cardiac troponin C (TNNC1): Implications for heart failure, cardiomyopathies, and troponin modulating drugs

Author: Monica X. Li,Peter M. Hwang
Publication: Gene
Publisher: Elsevier
Date: 25 October 2015

Order Completed

Thank you for your order.

This Agreement between Sam Julien ("You") and Elsevier ("Elsevier") consists of your license details and the terms and conditions provided by Elsevier and Copyright Clearance Center.

Your confirmation email will contain your order number for future reference.

License Number	5257340762058
License date	Feb 27, 2022

Printable Details

Licensed Content

Licensed Content Publisher	Elsevier
Licensed Content Publication	Gene
Licensed Content Title	Structure and function of cardiac troponin C (TNNC1): Implications for heart failure, cardiomyopathies, and troponin modulating drugs
Licensed Content Author	Monica X. Li,Peter M. Hwang
Licensed Content Date	Oct 25, 2015
Licensed Content Volume	571
Licensed Content Issue	2
Licensed Content Pages	14

Order Details

Type of Use	reuse in a thesis/dissertation
Portion	figures/tables/illustrations
Number of figures/tables/illustrations	1
Format	electronic
Are you the author of this Elsevier article?	No
Will you be translating?	No

Controlling the Synthesis and Assembly of Silver Nanostructures for Plasmonic Applications

Author: Matthew Rycenga, Claire M. Cobley, Jie Zeng, et al
Publication: Chemical Reviews
Publisher: American Chemical Society
Date: Jun 1, 2011

PERMISSION/LICENSE IS GRANTED FOR YOUR ORDER AT NO CHARGE

This type of permission/license, instead of the standard Terms and Conditions, is sent to you because no fee is being charged for your order. Please note the following:

- Permission is granted for your request in both print and electronic formats, and translations.
- If figures and/or tables were requested, they may be adapted or used in part.
- Please print this page for your records and send a copy of it to your publisher/graduate school.
- Appropriate credit for the requested material should be given as follows: "Reprinted (adapted) with permission from {COMPLETE REFERENCE CITATION}. Copyright {YEAR} American Chemical Society." Insert appropriate information in place of the capitalized words.
- One-time permission is granted only for the use specified in your RightsLink request. No additional uses are granted (such as derivative works or other editions). For any uses, please submit a new request.

If credit is given to another source for the material you requested from RightsLink, permission must be obtained from that source.

BACK CLOSE WINDOW

SERS: Materials, applications, and the future

Author: Bhavya Sharma,Renee R. Frontiera,Anne-Isabelle Henry,Emilie Ringe,Richard P. Van Duyne
Publication: Materials Today
Publisher: Elsevier
Date: January–February 2012

Order Completed

Thank you for your order.

This Agreement between Sam Julien ("You") and Elsevier ("Elsevier") consists of your license details and the terms and conditions provided by Elsevier and Copyright Clearance Center.

Your confirmation email will contain your order number for future reference.

License Number	5257340425217
License date	Feb 27, 2022

Printable Details

Licensed Content

Licensed Content Publisher	Elsevier
Licensed Content Publication	Materials Today
Licensed Content Title	SERS: Materials, applications, and the future
Licensed Content Author	Bhavya Sharma,Renee R. Frontiera,Anne-Isabelle Henry,Emilie Ringe,Richard P. Van Duyne
Licensed Content Date	January–February 2012
Licensed Content Volume	15
Licensed Content Issue	1-2
Licensed Content Pages	10

Order Details

Type of Use	reuse in a thesis/dissertation
Portion	figures/tables/illustrations
Number of figures/tables/illustrations	1
Format	electronic
Are you the author of this Elsevier article?	No
Will you be translating?	No